D5.1 EXPERIMENTAL INVESTIGATION IN COUNTERFLOW MODEL FLAMES

Document Information

Contract Number	821418
Project Website	www.estimate-project.eu
Contractual Deadline	M39
Dissemination Level	PUBLIC
Nature	Report
Author	Petros Vlavakis (KIT)
Contributor(s)	
Reviewer	Daniel Mira Martínez (BSC)
Keywords	Model flames, counterflow diffusion flames, PAHs, soot, high pressure laminar flames, jet-A1-surrogate

Change Log

The research leading to these results has received funding from the Clean Sky 2 Joint Undertaking under the European Union's Horizon 2020 research and innovation programme under grant agreement No. 821418.

Version	Author	Description of Change
V0.1	Petros Vlavakis	Initial draft
V0.2	Daniel Mira	Full review
V1.0		Final version

Table of Contents

1. Executive Summary

This document provides a summary of the experimental activities performed at the Engler-Bunte-Institute at the Chair of Combustion Technology (EBI-Vbt) at the Karlsruhe Institute of technology (KIT) in the framework of the ESTiMatE project. Scope of the project is to develop a modelling strategy for the prediction of emissions in jet engine applications. In this context, different working packages were agreed in order to meet this target. EBI-Vbt is involved in the Working package (W.P.) 5.1. Focus of this W.P. is to generate and deliver unique experimental data sets from laminar counterflow model flames under well-defined conditions including data for temperature, gaseous species concentration profiles and soot formation, in order to facilitate the development of the chemical kinetic and soot models. For this purpose, a counterflow burner was used.

In the framework of ESTiMatE it was decided that the investigations in W.P. 5.1 will mainly focus on non-premixed counterflow flames of ethylene, ethylene doped with the surrogate A and the pure surrogate A. Surrogate A is a four component kerosene surrogate developed from USTUTT for the purposes of the ESTiMatE project. However, during the project period it was realised that there is not only a lack of data for multi component fuels as the surrogate A chosen in ESTiMatE, but also in the data available for the single components of the surrogate A. For this reason, in order to increase the accuracy and the performance of the developed models, investigations in non-premixed counterflow flames of the single components of the surrogate A like iso-octane and trimethylbenzene have been performed.

For the investigations in the atmospheric and high pressure non-premixed counterflow flames the following measurement techniques and procedures were developed and applied. The temperature acquisition was performed with a constant tension thermocouple developed and constructed at KIT. The species concentration profiles were determined via gas chromatography, where the samples were taken from the flame with a sampling system designed special for the geometry of the used burner. The soot formation characteristics of the flames were examined with two different laser measurement techniques. The sooting limits of the different fuels and the surrogate A were examined with the laser scattering technique, while the determination of the soot volume fraction and the primary particle size distributions were determined with the laser induces incandescence technique (LII).

In the following report all aforementioned procedures and techniques will be presented and explained in detail.

2. Introduction

With the years, the legislation for emissions from combustion systems are becoming stricter. In the Aviation sector the main concern was on Greenhouse Gas Emissions (GGE), however new particulate matter standard for aircraft engines come into force [1]. Despite GGE, aircraft engines emit also soot particles that have also an impact on climate change and human health [2]. These are formed both on the ground and at cruising altitudes, where they act as condensation nuclei for ice crystals, resulting in the formation of contrails, which may linger in the sky as contrail cirrus clouds [3]. Hence, the reduction of soot emissions from the aviation sector is essential.

The ESTiMatE Project aims to develop a modelling strategy for the accurate prediction of emissions in jet engine applications. To tackle this challenge different working packages where accomplished including experimental and numerical investigations in order to develop a tool which will be able to predict accurately soot particle emissions from jet engines.

Accurate prediction of soot emissions requires a detail understanding of how soot is produced in engine combustion chambers. The soot formation process is a very complex phenomenon and in order to clarify the reasons that lead to the formation of soot particles, simplified experiments in model-flames with well-defined boundary conditions uncoupled from engine complexity are from high importance.

In W.P.5.1 at the EBI-Vbt of the KIT fundamental experiments in one dimensional model flames of various fuels have been performed to address this aforementioned challenge. In this context, non-premixed counterflow flames of ethylene, ethylene doped with a jet surrogate and the pure jet surrogate have been investigated. From the investigations at the EBI-Vbt unique experimental data sets from laminar counterflow model flames at different pressure levels, including temperature profiles, gaseous species concentration profiles and data regarding soot formation have been delivered. Scope of this W.P. is to facilitate the development of the chemical kinetic and soot models and increase their performance for complex fuels.

Target of the ESTiMatE consortium is the development of an accurate emissions prediction model for jet engine application. Real kerosene is a very complex multi component fuel and at the same time, the composition varies depending on the location. In order to develop a chemical kinetic model for jet engine applications someone has to make some compromises regarding the fuel composition for which the model will be developed and validated. In the ESTiMatE project it was decided that a four component surrogate will be used. The surrogate A (this is the name of the kerosene surrogate in the ESTiMatE project) contains one representative component from each of the main species

groups that can be found in real kerosene (alkanes, iso-alkanes, cycloalkanes and aromatics). The composition of the surrogate A was chosen by our project partner USTUTT, who is responsible for the development of the chemical kinetic model, in order to have similar chemical and physical properties to real kerosene. The volume composition of the surrogate A is presented in Table 1.

Table 1: Composition of the Surrogate A composition

group	Component	Composition in Vol.-%
alkanes	n-Dodecane	52.0%
iso-alkanes	iso-Octane	15.8%
cycloalkanes	Cyclohexane	12.1%
aromatics	Trimethylbenzene 1,3,5	20.2%

During the project period it was realised that there is not only a lack of data for multi component fuels as the surrogate A chosen in ESTiMatE, but also in the data available for the single components of the surrogate A. For this reason, in order to increase the accuracy and the performance of the developed models, investigations in non-premixed counterflow flames of the single components of the surrogate A like iso-octane and trimethylbenzene have been performed.

For the aforementioned investigations in the atmospheric and high pressure non-premixed counterflow flames at the EBI-Vbt at the KIT two different counterflow setups were used. One test rig was used for the investigations under atmospheric pressure and the other one was used in order to investigate the influence of pressure on flame structure. At the same time different measurement techniques have been developed in order to measure accurate and with a sufficient resolution the temperature field, the species concentration profiles, especially the for the PAHs, and soot formation. The temperature acquisition was performed with a constant tension thermocouple developed and constructed at KIT. The species concentration profiles were determined via gas chromatography, where the samples were taken from the flame with a sampling system designed special for the geometry of the used burner. The soot formation characteristics of the flames were examined with two different laser measurement techniques. The sooting limits of the different fuels and the surrogate A were examined with the laser scattering technique, while the determination of the soot volume fraction and the primary particle size distributions were determined with the laser induces incandescence technique (LII).

In the next sections of this report the used setups and the developed and applied measurement techniques will be presented in detail. Following to that, the gained experimental results will be presented. The presentation of the results is separated in two sections. The first section contains three different parts. In the first part experimental results regarding temperature and gaseous species profiles gained from one iso-octane non-sooting non-premixed counterflow flame will be presented and compared with

numerical results from different already available kinetic models. In this part of the report, the differences between the available mechanisms and the experimental results will be highlighted showing the lack of data from counterflow flames of complex fuels. In the second part, experimental data regarding temperature, gaseous species concentration profiles and soot formation from the examined iso-octane flames will be presented in detail. The last part of this chapter presents the list of all investigated flames used for the development and validation of the kinetic and soot models. In the second section the investigated flames under pressure will be presented.

3. Experimental setup and procedures

In the following the experimental setups and procedures used in these investigations will be explained in detail. First, the counterflow setup and the developed measurement techniques used in the investigations under atmospheric conditions will be presented followed by the setup and the developed measurement techniques used in the investigations under high pressure.

3.1 Counterflow setup for model flame investigations under atmospheric pressure

All experimental investigations at atmospheric pressure were performed with the counterflow burner presented in Figure 1. The used burner is designed and built according to the design developed by Prof. Seshadri's group at the University of California in San Diego [4]. The complete setup is presented in Figure 1.

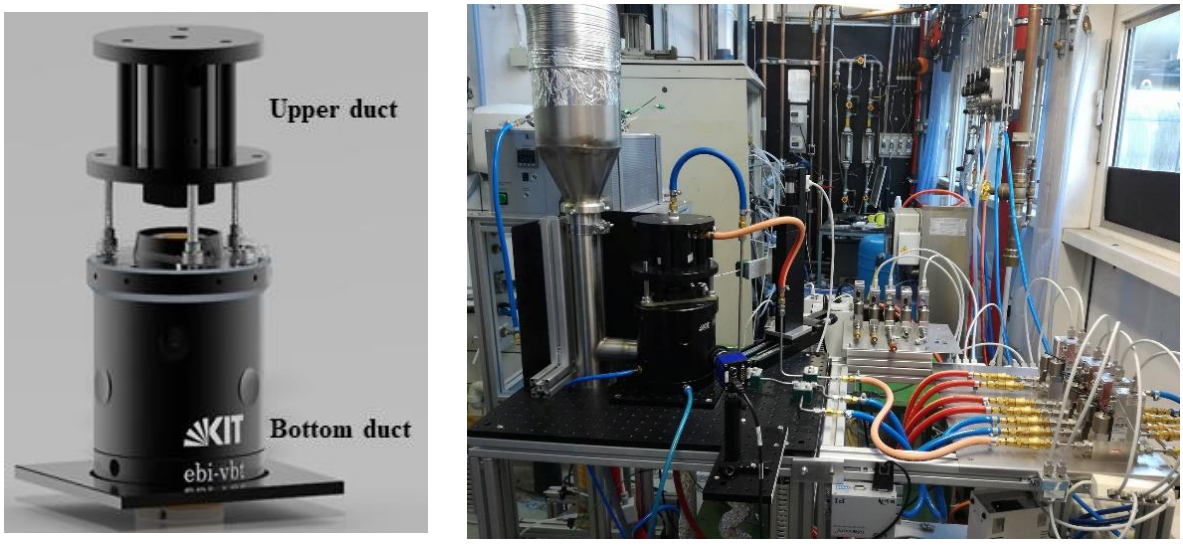

Figure 1: Counterflow burner (left) and setup (right) at the EBI-Vbt at the KIT for investigation under atmospheric pressure.

Core of this setup is the counterflow burner. However, the setup also consists of several

components required to perform combustion experiments with both gaseous and liquid fuels. To provide the burner with the desired fuel mixture, all gaseous components are supplied from high-pressure cylinders and their flow rates are controlled by calibrated thermal mass flow controllers (MFCs), as shown in the flow diagram in Figure 2. Liquid fuels are supplied with a liquid fuel preparation system consisting of a syringe pump and a direct vaporizer. All fuel lines are heated to prevent condensation in the fuel stream and the burner body.

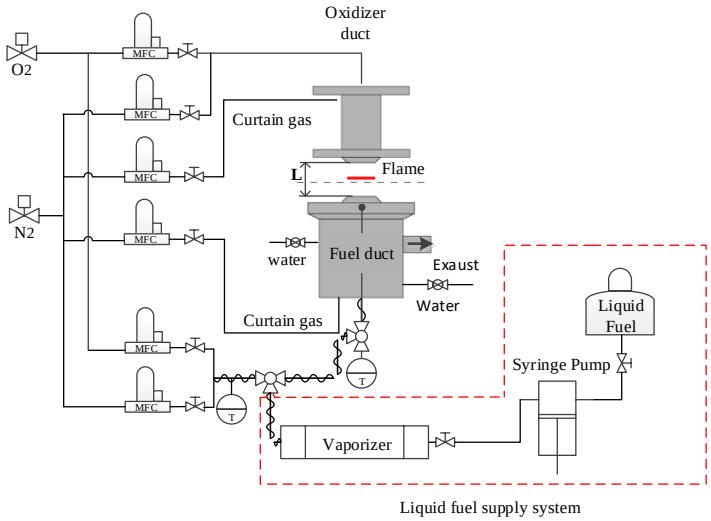

Figure 2: Flow diagram of the counteflow experimental setup at the EBI-VBT.

Figure 3 shows the flow field of a counterflow burner. As can be seen, in the case of a counterflow flame there is not only one reacting mixture, but two. The mixture that flows through the lower tube labelled (1) and the mixture that flows through the upper tube labelled (2). ? not labelled in picture. Also no fuel line to upper tube. The symbols used to represent the mixtures are shown in **Fehler! Verweisquelle konnte nicht gefunden werden.**. ? reference

When stabilizing the flames on the counterflow burner, a very important role is also played by the velocities of both flows, which are calculated by equations (1) and (2).

$$u_1 = \frac{\dot{V}_1}{A_{duct}} \quad (1)$$

$$u_2 = \frac{\dot{V}_2}{A_{duct}} \quad (2)$$

Where the supplied volume flows and A denotes the area of the respective duct.

Another parameter defining the flow ratio at the counterflow burner is the aspect ratio (α_2)

calculated from equation (3). The strain rate, which is defined at the oxidizer side, is a quantity that depends on the flow velocities and is used as a dimensionless quantity to represent the flow field independent of the geometrical properties of the burner.

$$a_2 = \frac{2u_2}{L}\left[1 + \frac{u_1\sqrt{\rho_1}}{u_2\sqrt{\rho_2}}\right] \tag{3}$$

Where ρ denotes the flow densities of the supplied volume flows.

Table 2: Symbols of the components in the flows of a counterflow burner.

Upper flow	
Mass fraction	Symbol
Oxygen mass fraction	$Y_{O2,2}$
inert gas mass fraction	$Y_{innert,2}$
Lower flow	
Mass fraction	Symbol
Fuel mass fraction	$Y_{F,1}$
inert gas mass fraction	$Y_{innert,1}$

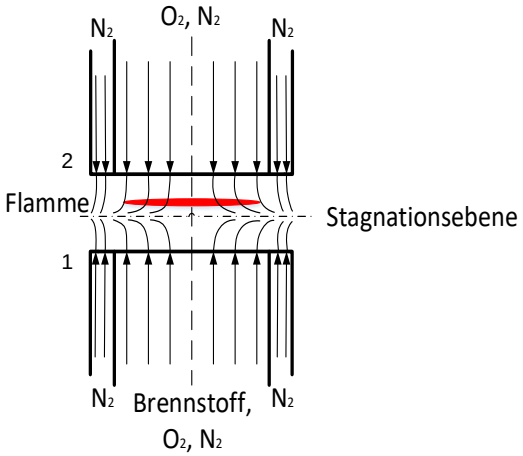

Figure 3: Flow field of a counterflow burner.

In the experiments performed a momentum balance is set, equation (4). Hence, the stagnation plane is placed midway between the two outlets.

$$\rho_1 u_1^2 = \rho_2 u_2^2 \tag{4}$$

By combining equations (3) and (4), equation (5) can be set up. In equation (5) the α_2 depends only on the velocity at the oxidizer boundary and in this way simplifies the calculations of the parameters mentioned above.

$$a_2 = \frac{4u_2}{L} \tag{5}$$

Another important parameter of a counterflow flame is the stoichiometric mixture fraction (ξ_{st}). The ξ_{st} has a value from zero to one ($0 < \xi_{st} < 1$) and is calculated by equation (6). This parameter determines the position of the flame between the two ducts. If $\xi_{st} = 0$, the

flame is at the oxidizer boundary and if ξ_{st} = 1, the flame is at the fuel tube exit.

$$\xi_{st} = \left(1 + \frac{\nu Y_{F,1}}{Y_{O_2,2}} \right) \tag{6}$$

3.2 Developed measurement techniques for investigations under atmospheric pressure

This part of the report details the measurement techniques used and the associated systems developed, such as thermocouples and sampling systems.

3.2.1 Temperature measurements via thermocouple

To perform the temperature measurements a new thermocouple probe was designed and constructed (Figure 4) [5]. A fine-wire (0.1 mm) S-type thermocouple with a built-in spring mechanism that places the wires under tension when necessary to prevent deformation in the flame region was used. The thermocouple wires and the bead (diameter of 0.4 mm) have been coated with zirconia to eliminate catalytic effects.

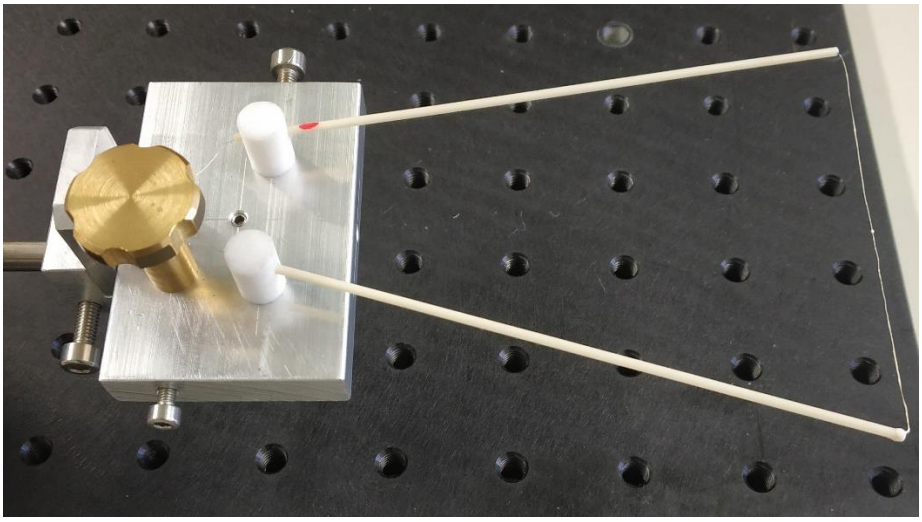

Figure 4: S-type tension thermocouple used for temperature measurements.

The measured flame temperatures were corrected for radiative losses following the procedure given by Shaddix [6 Shaddix].

$$T_{corrected} = T_g + \sigma \epsilon T_g^4 \left(\frac{d_{bead}}{\lambda Nu}\right)$$

Where, emissivity ε = 0.4, the Boltzmann constant σ = 5.67 x 10^{-8} W/m^{2}K^4, Nusselt number Nu is assumed to be constant at 2.0, and λ denotes the temperature dependent thermal conductivity of the wire,

$$\lambda = 4.6942 \times 10^{-3} + 8.1225 \times 10^{-5} T_g - 1.4547 \times 10^{-8} T_g^2$$

where, T_g stands for gas temperature. The uncertainty in the reported temperature is max ±70 K, taking into account the standard deviation and the uncertainties introduced due to the radiation correction procedure.

3.2.2 Species concertation profile measurements via Gas Chromatography

A GC-MS system from the company Teckso with a heated storage valve oven, which can be seen in Figure 5, was used to determine the species concentrations in the counterflow non-premixed flames. To analyze the samples, the system contains three detectors and a mass spectrometer. The GC uses a thermal conductivity detector for the detection of the following major species (H_2, CO, CO_2, O_2, N_2) and two flame ionization detectors (FIDs) for the detection of hydrocarbons. The first FID is used for the detection of hydrocarbons up to C6 and the second for the detection of all hydrocarbons with more than 6 carbon atoms.

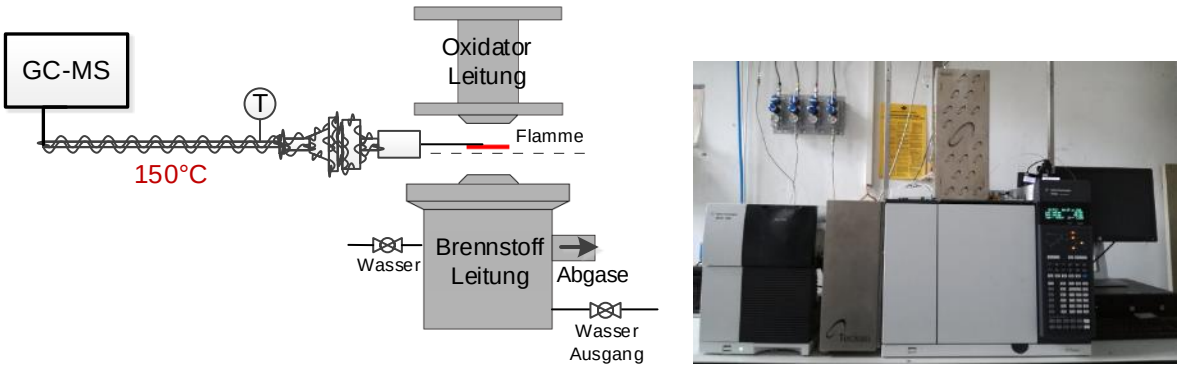

Figure 5: GC-MS and probing system for measuremetns of gaseous species concentration profiles form non-premixed counterflow flames

The gas sample is taken from the flame by means of a ceramic tube (inner diameter 0.3 mm) from the desired position. The ceramic tube has a length of about 25 mm. After the ceramic, the gas is led through a metal tube (inner diameter 1.6 mm) to the GC-MS

system. The complete transfer line is tempered to a temperature of approx. 150°C to avoid condensation of the gas components. In addition, a filter is integrated in the transfer line to remove solid particles (e.g. soot) that could damage the GC-MS system. The used gas probing system is presented in Figure 5. The maximum total error in measured concentrations is about 10% for the major species (such as H_2, CO_2, CO, etc.,) and the first hydrocarbons and 20% - 40% for the higher hydrocarbons and PAHs.

3.2.3 Measurement techniques for the determination of soot

For the determination of the sooting tendency and the soot formation process in the examined flames two non-intrusive laser measurement techniques have been applied. The laser scattering technique is used in order to determine the sooting tendency of the different used fuels and to characterize which flame parameters lead to soot formation. For the characterization of the soot formation process the laser induced incandescence (LII) technique was applied.

Laser Scattering

For the determination of the sooting limits for the fuels of interest I the framework of the ESTiMatE project the setup presented in Figure 6 was used. The applied method follows the measurement principle used by Joo et al. [7] for determining sooting limits in counterflow non-premixed flames of ethylene/propene mixtures and by Wang and Chung [8] in alkanes and alkenes non-premixed counterflow flames.

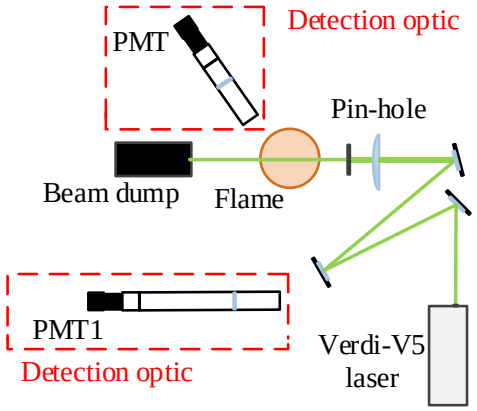

Figure 6: Scattering setup for determination of sooting limits in counterflow flames

For the determination of the soot limits a continuous wave diode pumped solid state laser at a wavelength of 532 nm and a power of 0.3 W was used. The laser beam was guided through the center of the burner via several of optical components. The scattering signal was captured with a photomultiplier tube. To reduce noise at the photomultiplier, a pinhole and a narrow band-pass filter (532 nm) were used. The intensity signals were recorded using lock-in amplifiers. Sooting limits were determined by comparing the scattering intensity from gas molecules and soot particles [7]. The applied methodology is presented

in Figure 7. In this graph, the normalized scattering intensity measured along a non-premixed counterflow flames with a fuel mass fraction of 0.40 is presented. As can be seen from Figure 7 at a strain rate of 100 s^{-1}, which is under non-sooting conditions, the scattering intensity decreases monotonically from the fuel to the oxidizer side due to increased temperature. By decreasing the strain rate the signal from soot particles interferes in the captured signal, resulting in a local maximum (α_2 = 45 s^{-1} in Figure 7). As α_2 is further decreased, this signal increases indicating a higher concentration of soot. All investigations have been performed with an increment of 1 in the strain rate. In the case present in Figure 7, the sooting limit is at α_2 = 45 s^{-1} having the accuracy of ±1 s^{-1}. The sooting limits of all fuels of interest were determined in the same manner.

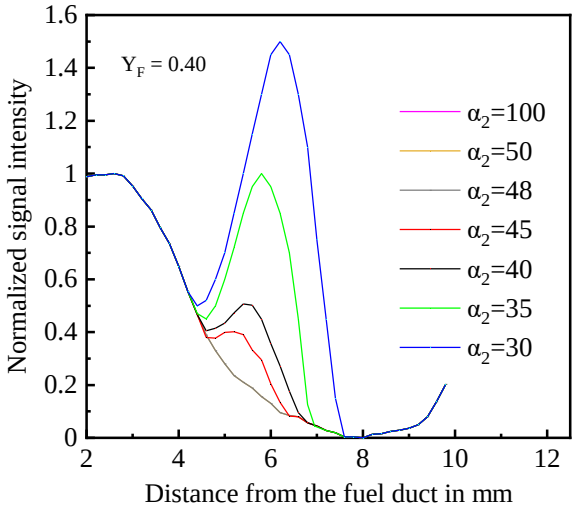

Figure 7: Normalized laser scattering signal versus the distance from the fuel duct for different strain rates and at a fuel mass fractions of 0.40 in iso-octane counterflow non-premixed flames.

Laser Induced Incandescence (LII)

Soot volume fraction and primary particle size distribution in the examined counterflow flames are determined via Time-Resolved Laser Induced Incandescence (TR-LII). The investigations were performed with the fundamental wavelength of a 10 Hz-pulsed Nd:YAG laser at 1064 nm. A rotating half-wave plate and a polarization beam splitter are used to provide a constant and defined energy density of the laser pulses. The central part of the Gaussian laser beam is selected using a ceramic diaphragm and a pinhole with a diameter of 1 mm before entering measuring volume. The time-resolved LII signal decays were collected at 120° angle to the laser beam using a lens system and two fast photomultipliers (trise = 0.5 ns) equipped with 10 nm FWHM band-pass interference filters centered at λ_d^i= 450 nm and λ_d^j=650 nm, respectively. A digital oscilloscope was used to record the signals and a fast photodiode was used to trigger the detection system as well as detect single laser pulse energies. The two-color TR-LII setup was calibrated against an SMPS using a spark-discharged soot aerosol. The used setup is presented in Figure 8.

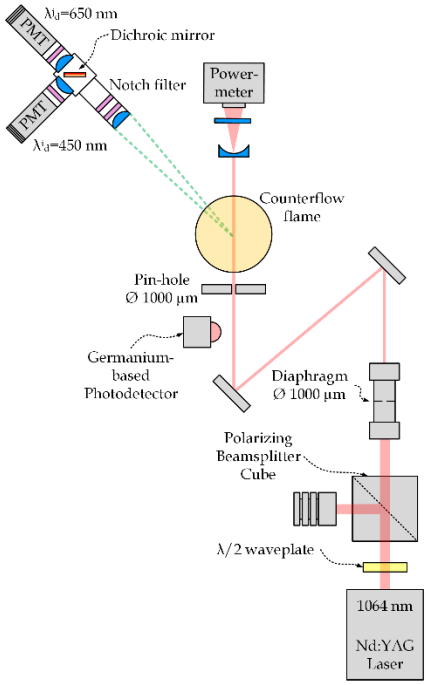

Figure 8: Schematic illustration of the optical setup for the 2 color TR-LII measurements.

3.3 Counterflow setup for model flame investigations under high pressure

In this part of the report the setup for the investigations under high pressure is presented (Figure 9). Core of this setup is the counterflow burner and the pressure chamber. However, many sub-components, like the traverse system, the gas regulation and feeding system, the pressure regulation unit, etc., are also very important in order to be able to perform experiments under high pressure. Some of the sub-components will be presented in the next paragraphs in detail.

First the used counterflow burner is presented. For the ESTiMatE project a scaled-down counterflow burner, presented in Figure 10, was used for the high-pressure experiments. The working principle of the smaller burner is similar to the burner used in the atmospheric experiments. The only important difference between the two systems is that the downsized burner has a duct diameter of 10 mm instead of 25 mm. The reduction in duct diameter results in a reduced fuel and oxidizer consumption especially at high pressure conditions. Hence, in a significant reduction in gas costs is achieved.

To be able to perform experiments under pressure, a high-pressure setup was designed and manufactured (Figure 11). The pressure chamber is built and certified for operation up to a maximum pressure of 10 bar. Optical access to the pressure chamber is provided by means of four quartz glass windows. The optical access allows us to perform measurements and also to monitor the flame continuously. The pressure chamber is also equipped with two flanges on the top and bottom to allow cleaning and maintenance of the burner. There are several inlet and outlet ports on the periphery of the chamber for

the supply of gases, mounting of temperature and pressure sensors, heating and cooling of the pressure chamber etc.

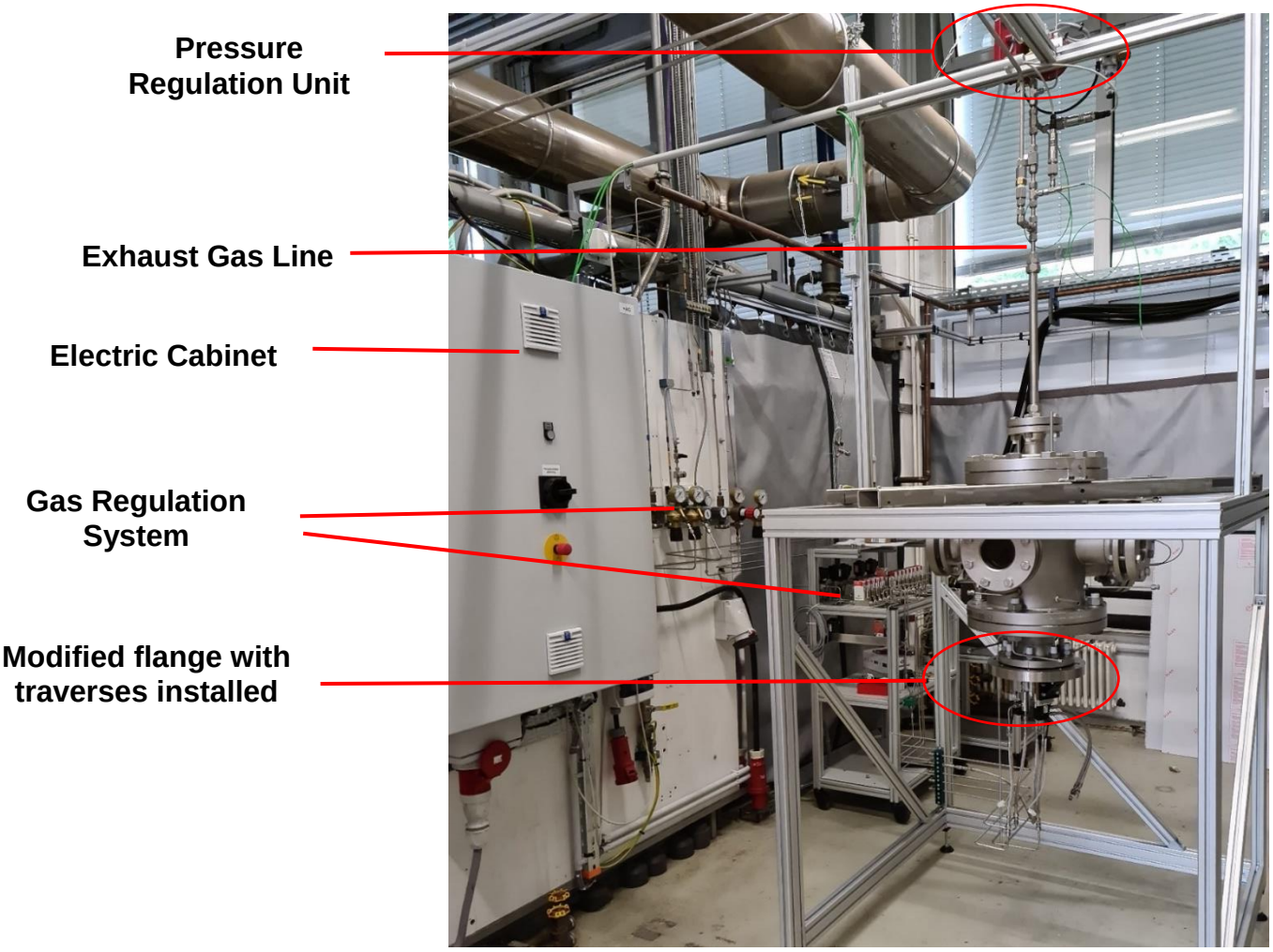

Figure 9: High pressure counterflow setup at KIT EBI-vbt.

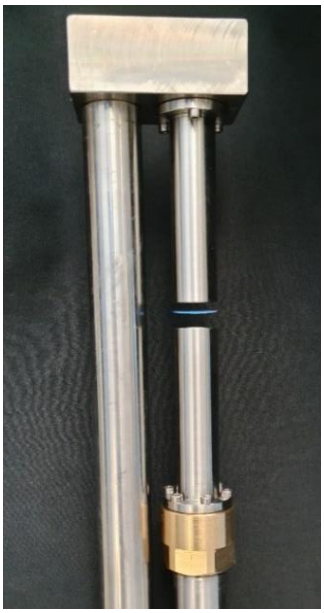

Figure 10: Counterflow burner for high pressure investigations.

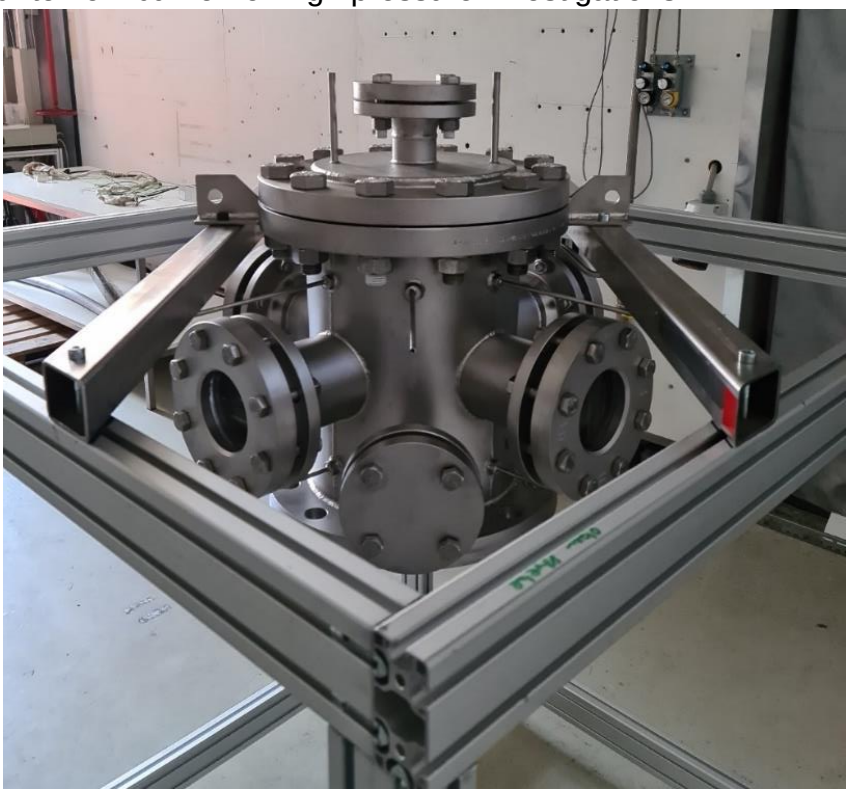

Figure 11: Pressure chamber for investigations under high pressure.

An important part of the assembly is the installation and movement of the burner in the pressure chamber. As shown in Figure 12, the burner is mounted on two cylindrical tubes, one carrying the fuel duct and the other the oxidizer duct. The movement of the two tubes is controlled by an electronic linear traverse and operated using a PC. A new separate

flange was fabricated and a special fixture was built to mount the tubes and associated fixtures to the pressure chamber (Figure 13).

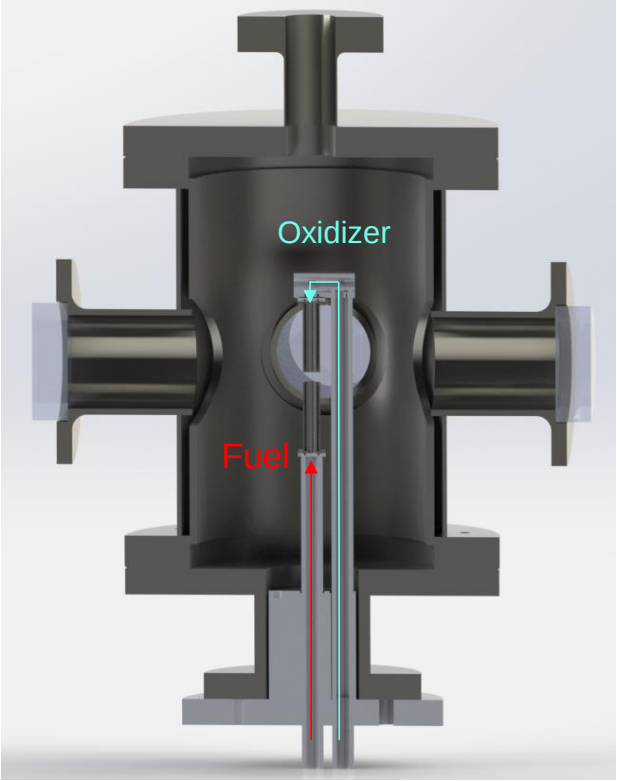

Figure 12: Cross section of the pressure chamber together with the burner.

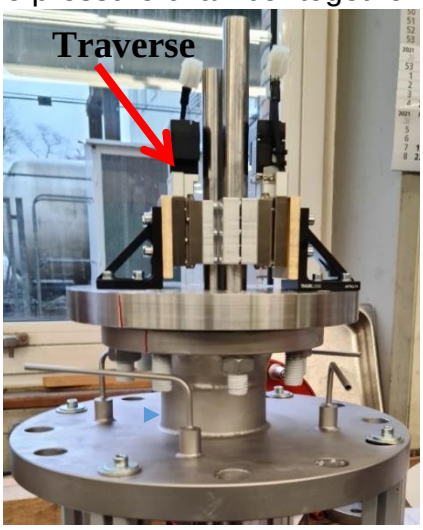

Figure 13: Assembly of the axes and the associated fixtures on the pressure chamber

Another important part is the design of the gas supply system for the fuel and oxidizer ducts. All gases are provided to the burner through the two tubes shown in Figure 12. However, both the ducts require two separate gas flows (reactant gas mixture and N_2 for

the curtain gas). For this reason, the design and construction of special parts to guide the separate flows from the inlet of the chamber to the outlet of the burner were of great importance. Due to the high demands on precision and accuracy, the required parts were manufactured using a CNC machine. Figure 14 shows the fabricated part for feeding gases on the oxidizer side.

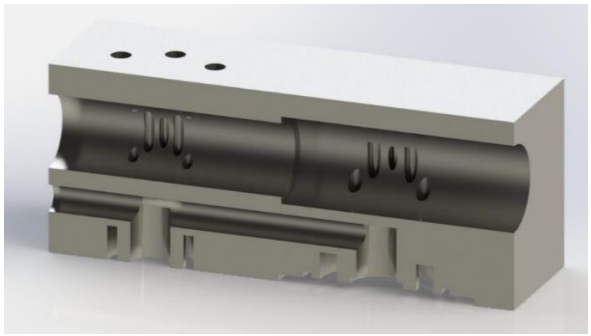

Figure 14: CNC machined part for feeding gases on the oxidizer side.

Figure 15 shows the assembled counterflow burner and its installation in the pressure chamber.

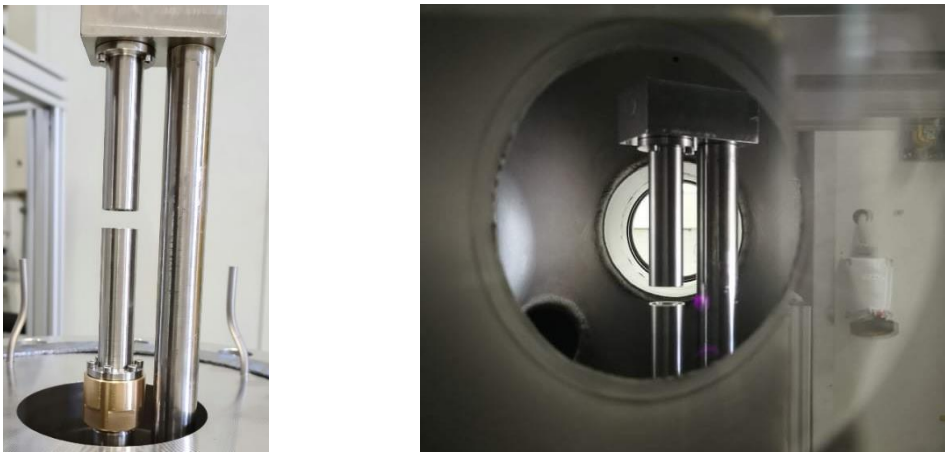

Figure 15: Assembled counterflow burner with feed system (Left); view of the burner from the optical access of the pressure chamber after installation (Right).

After mounting the burner inside the chamber, the ignition unit was installed. A Honeywell Q3200U silicon nitride surface igniter was used to ignite the burner. The installed igniter is shown in Figure 16.

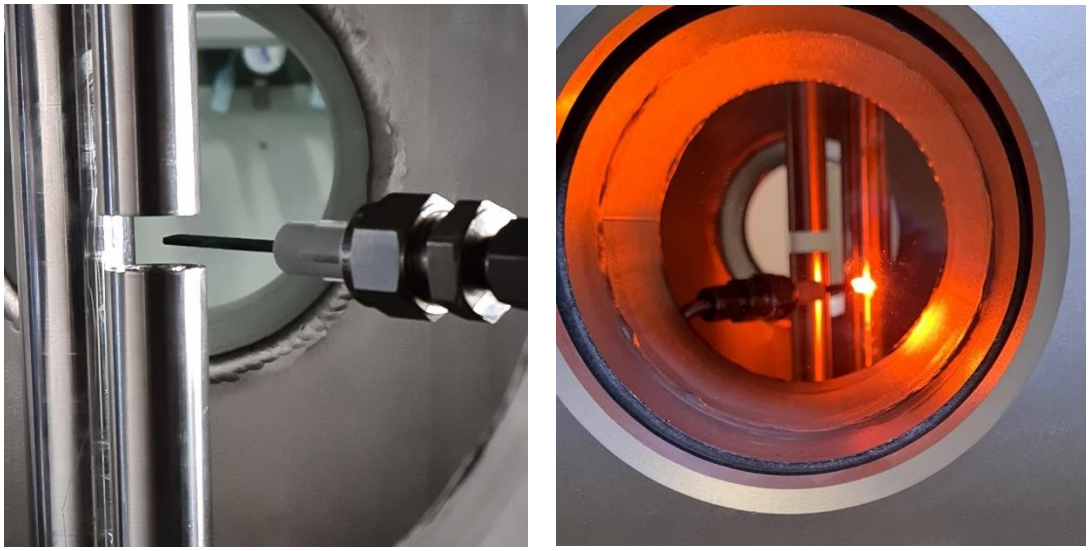

Figure 16: Installation of the igniter in the pressure chamber (left); testing of the ignition system (right).

The final step in completing the pressure setup was the installation of the following major sub-systems:

- Exhaust gas line
- Installation and testing of the gas supply lines
- Installation, testing and commissioning of the electrical cabinet
- Commissioning of the scaled-down counterflow burner under atmospheric conditions (Figure 17)

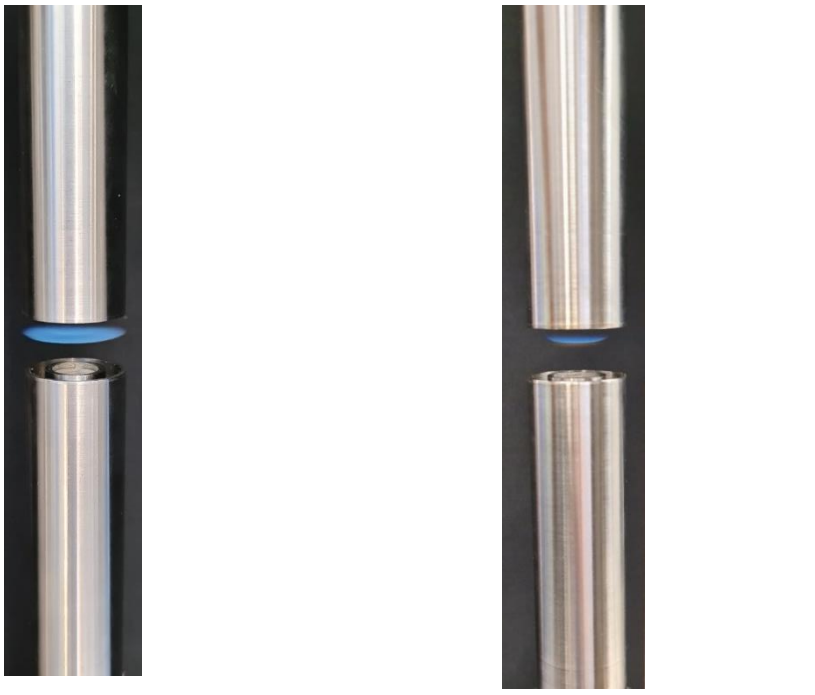

C_2H_4 Flamme at $Y_F = 0.3$ and $\alpha_2 = 200\ s^{-1}$

CH_4 Flamme: $Y_F = 0.3$, $\alpha_2 = 60\ s^{-1}$

Figure 17: Commissioning of the new counterflow burner.

After the high pressure test rig went successfully in operation at atmospheric conditions the experimental campaign for the investigation of the influence of pressure on flame structure have started. In the next chapter the development of the sampling probe system for GC measurements under high pressure will be presented. Following to that, in chapter 4 the boundary conditions and the experimental results from the high pressure flames will be resented.

3.4 Developed measurement techniques for investigations under high pressure

The main focus in the high pressure experiments is to measure the species concentration profiles at different pressure levels in order to facilitate the validation of the developed chemical kinetic model under high pressure conditions. In this context at EBI-Vbt a new sampling system was designed in order to extract gas probes from the pressure chamber and analyse them in the same GC-MS system used also in the atmospheric experiments. The propping system is presented in detail in the following paragraph.

3.4.2 Species concertation profile measurements via Gas Chromatography

For species measurements under pressure, a new sampling probe, leading the gas probe from the burner outside of the pressure chamber and to the GC-MS system (Figure 18) was constructed. The constructed probing system consists of two tubes inserted into one another. In the inner tube the gas probe is flowing from the burner to the GC-MS. At the same time, in the outer tube hot oil at 150°C flows to avoid condensations of the probed species in the line. The sample is taken through a ceramic tube similar to this used in the atmospheric flames. The ceramic tube used in these investigations had an inner diameter of 0.2 mm and a length of 10 mm and is mounted on the metallic tube shown in Figure 18. The metallic probe is mounted in the chamber through one of the windows. To facilitate this, one glass window is replaced with a metal part fitted with a pressure seal. At the end of the metallic tube Figure 19 shows the probe installed inside the chamber.

Figure 18: Probing system for gas species concentration measurements at the high pressure counterflow setup

Figure 19: Probing system for gas species concentration measurements at the high pressure counterflow setup mounted in the pressure chamber

4. Experimental results from non-premixed counterflow

As presented at the beginning of the report, the task of the EBI-Vbt is to generate a detailed experimental database from non-premixed counterflow flames from various fuels to facilitate the development of the chemical kinetic mechanism and the soot models. In the next part of the report the boundary conditions of the examined flames will be presented together with the gained results.

The experimental data generated at EBI-Vbt will be used and presented in the reports of the project partners involved in the development of the chemical kinetic mechanism and the soot models. Hence, in this report exemplary experimental results showing the importance of the performed measurements and their detection capabilities, will be presented.

In the next sub-chapters the characterization of iso-octane non-premixed counterflow flames at atmospheric pressure containing experimental results regarding temperature, gaseous species profiles and soot will be presented. In the first part, results from one non-sooting iso-octane non-premixed counterflow flame will be presented and compared with numerical results from different already available kinetic models. The differences between the available mechanisms and the experimental results will be highlighted showing the lack of data in counterflow flames of iso-octane. Following to that, experimental results showing the influence of the fuel mass fraction and strain rate on

temperature, gaseous species profiles and soot formation are presented. Here the main scope of the authors is to present the capability of the designed systems to capture the differences in the temperature, gas species profiles concentrations and soot formation even by small changes in the flame parameters.

In the last part of this chapter a list of all investigated flames at atmospheric and high pressure conditions used for the development and validation of the chemical kinetic and soot models are presented.

4.1 Iso-octane non-premixed counterflow flames at atmospheric pressure

As mentioned previously it was necessary to investigate flames from the individual components of the surrogate A. Thus, our investigations started with iso-octane. The focus of these measurements is to characterize the flame structure and soot formation of iso-octane non-premixed counterflow flames. The boundary conditions of the examined flames are presented in Table 3.

Table 3: Investigated non-premixed iso-octane counterflow flames at atmospheric conditions

Iso-octane non-premixed flames					
		Fuel side		Oxidizer side	
Flames	α_2 (s^{-1})	$Y_{C8H18,1}$	$Y_{N2,1}$	$Y_{O2,2}$	$Y_{N2,2}$
1	60	0.35	0.65	0.233	0.767
2	60	0.47	0.53	0.233	0.767
3	60	0.50	0.50	0.233	0.767
4	60	0.60	0.40	0.233	0.767
5	100	0.60	0.40	0.233	0.767
6	120	0.60	0.40	0.233	0.767

The results gained form the examined flames presented in Table 3 will be presented in three individual parts. In the first part, experimental results gained from flame 1 (non-sooting flame) shown in Table 3 will be compared with results from the 1-D simulations with available chemical kinetic models. The used kinetic models are listed in Table 4. Following to that, the second and third part present the influence of fuel mass fraction and strain rate on temperature, species concentration profiles and soot formation respectively. All experimental results for temperature, species concentration profiles and soot are presented as a function of the distance from the fuel duct.

4.1.1 Performance of available chemical kinetic models on non-premixed counterflow flames

As mentioned before, first a detail comparison between experimental results generated in ESTiMatE at the EBI-Vbt at KIT and different available chemical kinetic mechanisms

will be presented. Figure 20 shows the measured temperature profile from flame 1 (Y_F = 0.35, α_2 = 60 s^{-1}) in comparison with numerical predicted temperature profiles using six different mechanisms. From the graph it is observed that all mechanisms are giving similar results regarding the shape of the flame and are in agreement with the experimental results. However, the predicted peak temperature in the flame varies between the mechanisms showing differences of more than 100 K. Nonetheless, all mechanisms predict a peak temperature close to the measured one.

Table 4: Used Mechanisms

Mechanism	Fuels	Developed for	Used Acronym	Reference
KAUST PAH Mech 1	C_{1-12}	n-decane, n-heptane, iso-octane, toluene	KM1	[9]
Iso-octane oxidation mech	C_{1-8}	n-heptane, iso-octane	BPP	[10]
Zhong and Zheng mech	C_{1-8}	Isooctane, n-heptane, ethanol	Z&Z	[11]
POLIMI PRF PAH Alcohols Ethers mechanism	C_{1-12}	Gasoline surrogate mixtures	Polimi tot	[12]
TPRF + Alcohols mechanism	C_{1-12}	Gasoline	TPRF+Alc	[13]
C1-C16 HT mechanism	C_{1-12}	Diesel & Jet-fuels	C1-C16	[14]
Caltech mechanism	C_{1-12}		Caltech	[15]

After presenting the measured temperature profiles the measured species concentration profiles are presented. The gained results are presented in Figure 21-24. Figure 21 shows measured and computed concentration profiles of the major species. It is observed that the consumption of reactants (C_8H_{18} and O_2) and production of main combustion products (CO_2 and H_2O) is well predicted by all mechanisms. In contrast, deviations between mechanisms can be observed in the formation of the major intermediate species H_2 and CO.

The quantified small hydrocarbons (C_1 to C_3) are shown in Figure 22. For all small hydrocarbons, similar deviations between mechanisms, such as in H_2 and CO concentrations, could be observed. From Figure 22 it is clear that, as the carbon atoms number increases the deviations between the mechanisms increase as well. Nonetheless, for all hydrocarbons detected at least one of the used mechanisms shows a very good agreement with the experimental values, showing that an accurate reaction path way for each of the reported species is available and leads to similar concentrations like measured ones.

After showing the performance of the used mechanisms on concentration prediction of the first hydrocarbons, the comparison between measured and predicted concentrations for higher species and the first soot precursors is presented. Concentration profiles of the measured higher species and the first soot precursors, starting from benzene (C_6H_6 (A1)) up to indene (C_9H_8) are presented in Figure 23. As it is clear for the following graphs not all species identified experimentally are included in all used mechanisms. This is the first

large difference noticed between the used mechanisms. When species are not included in the mechanism, they are not taken into account in the used reaction paths. In this way their absence influences significantly the concentration of higher species and hence the formation of soot. As it is an important information for the performance of the mechanism whether a species is included in which mechanism or not, , a mechanism is excluded from the legend of the respectively graph if it does not include that particualar species. For example, in the graph presenting the concentration profile of the xylene isomers, only the mechanisms Polimi_tot and the C1-C16 mechanism are presented as they are the only mechanisms calculating the formation of xylene. As expected, from the results of the major species and the first hydrocarbons, the deviations between the used mechanisms increase for the higher hydrocarbons. The highest deviations can be found in the predicted concentration of benzene (A1) where the differences between the mechanisms are almost in the range of one order of magnitude. Similar deviations to benzene can be observed for all one aromatic ring species presented in Figure 23.

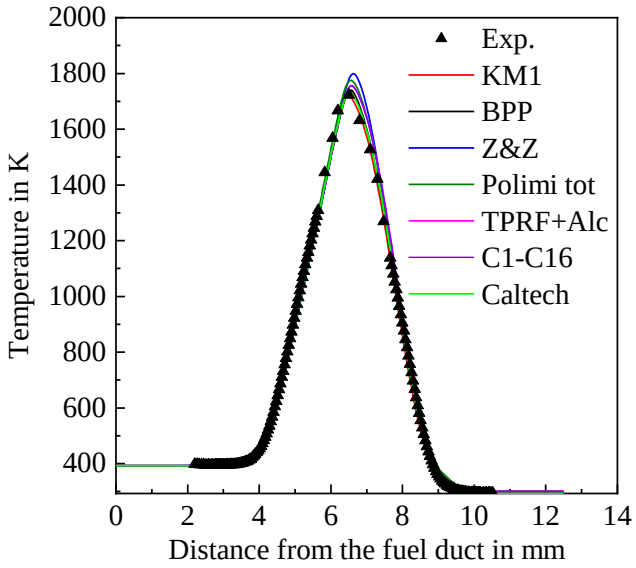

Figure 20: Measured (symbols) and predicted (solid lines) temperature profiles of a non-premixed iso-octane counterflow flames versus Distance from the Fuel Duct (DFD) at a strain rate of 60 s^{-1} ad a fuel mass fraction of 0.35.

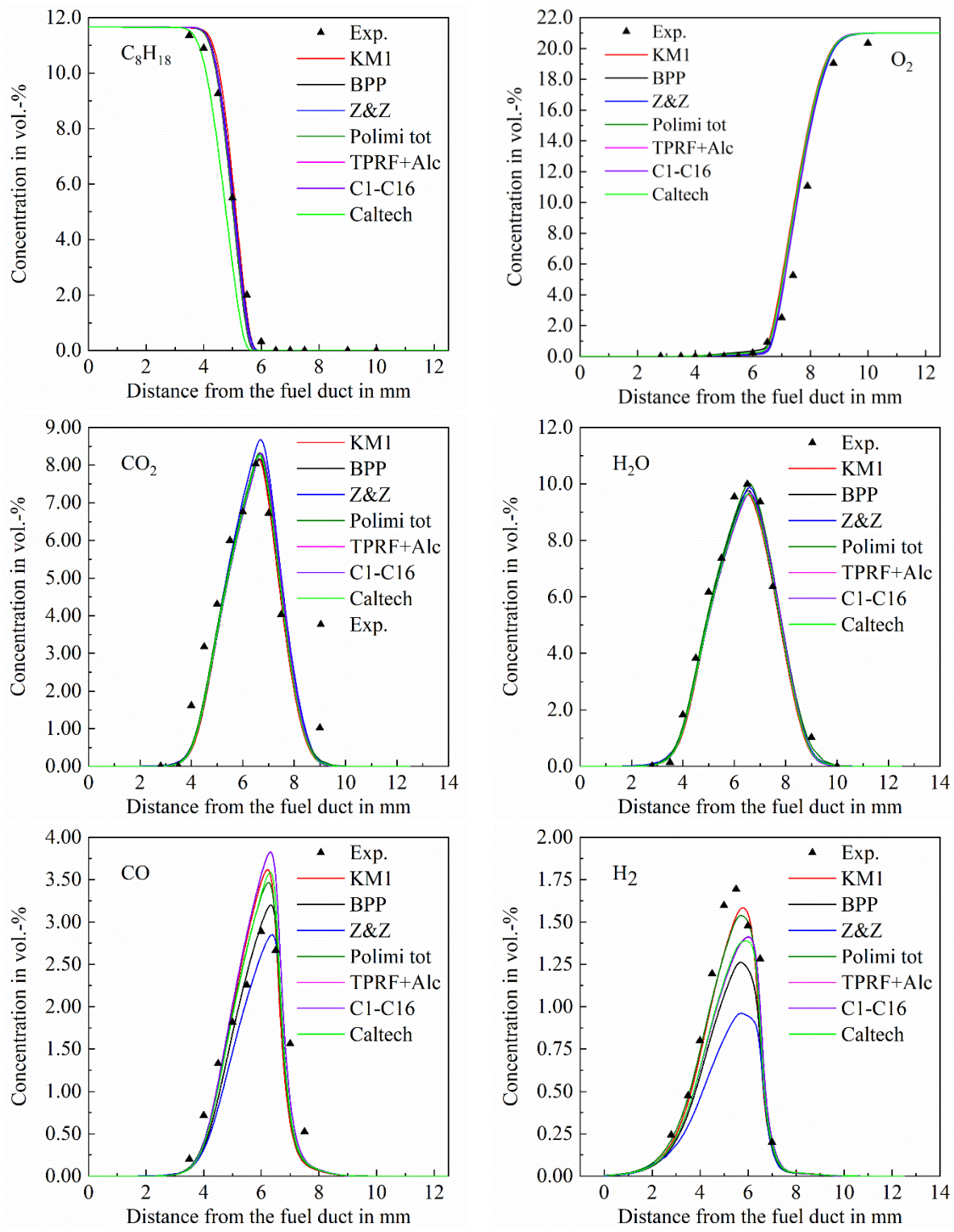

Figure 21: Measured (symbols) and computed (solid lines) concentration profiles of C_8H_{18}, O_2, CO_2, H_2O, CO and H_2 versus Distance from the Fuel Duct (DFD) in a non-premixed iso-octane counterflow flame.

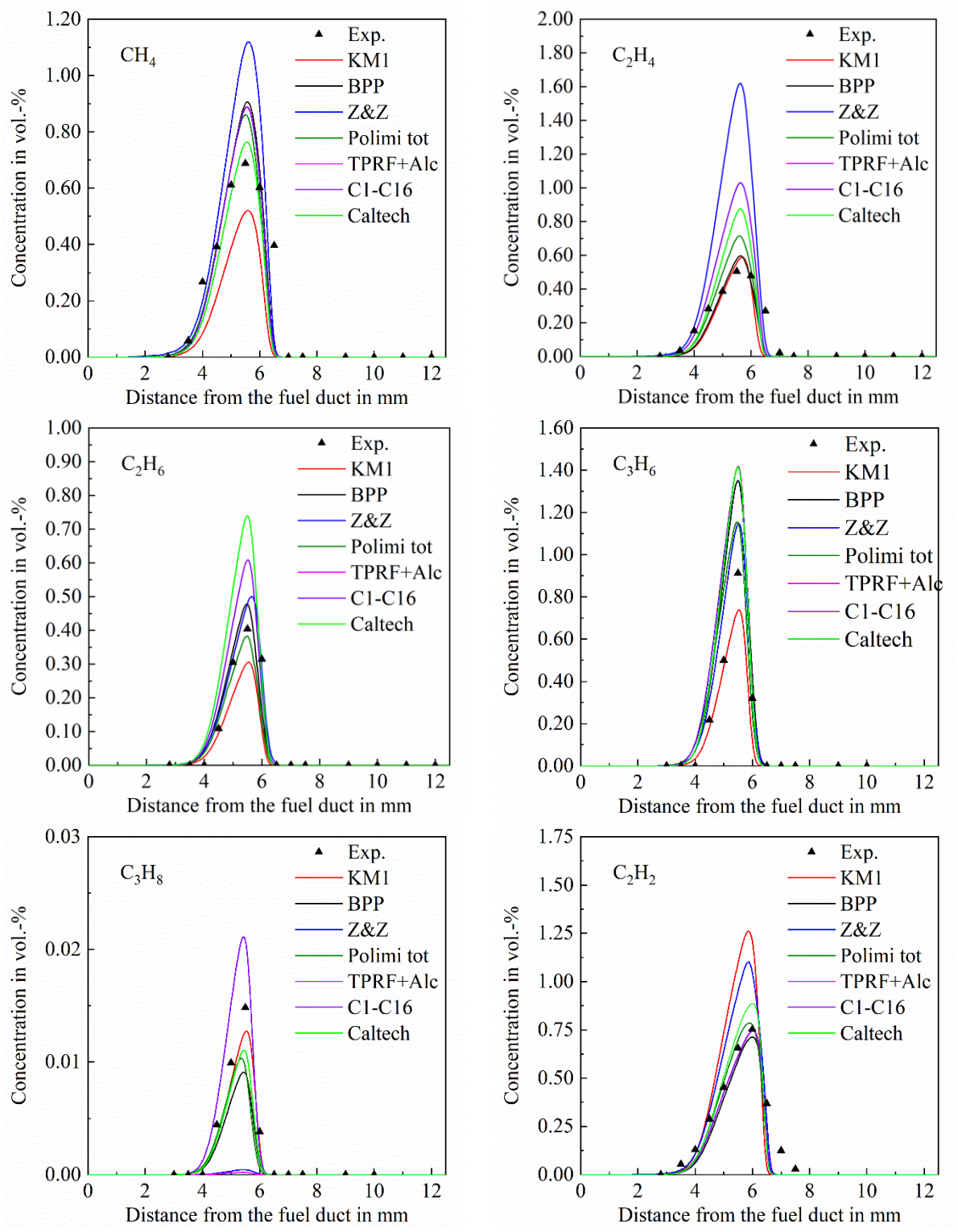

Figure 22: Measured (symbols) and computed (solid lines) concentration profiles of small hydrocarbons versus Distance from the Fuel Duct (DFD) in a non-premixed iso-octane counterflow flame.

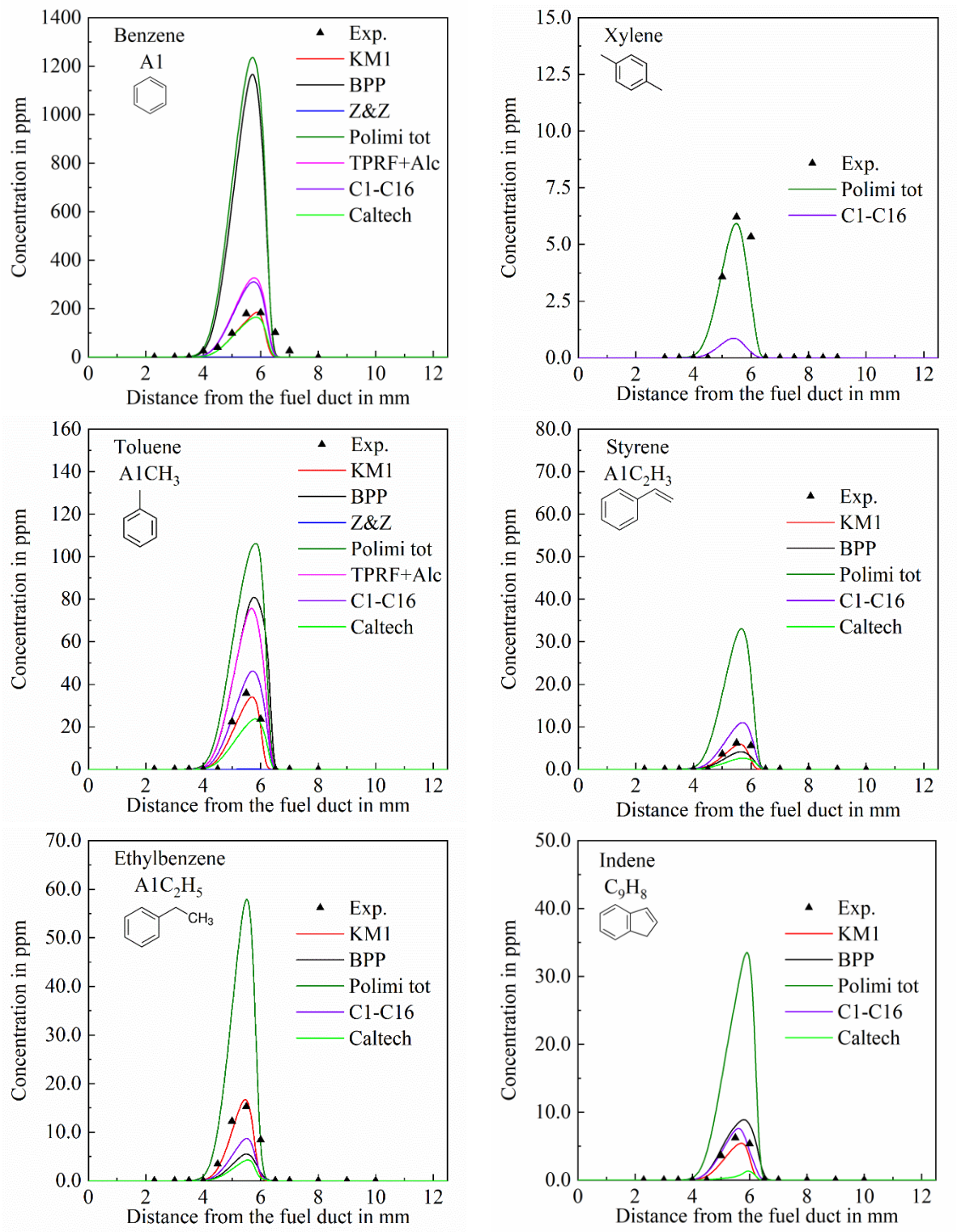

Figure 23: Measured (symbols) and computed (solid lines) concentration profiles of aromatics and PAHs versus DFD in a non-premixed iso-octane counterflow flame.

After presenting the measured soot precursors with one aromatic ring, Figure 24 shows the measured higher soot precursors and PAHs. For these species similar behaviour to

the ones presented in the previous figures can be observed. The experimental results show a very good resolution of the shape and have a good agreement with at least one of the used mechanism, almost for all four species presented in Figure 24. However, similar differences like in the above reposted species can be observed also for all the PAHs measured. The significant differences between the mechanisms shown in Figure 21-Figure 24, strengthen the conclusion that there is a lack of data in counterflow flames and especially for higher hydrocarbon species and soot precursors.

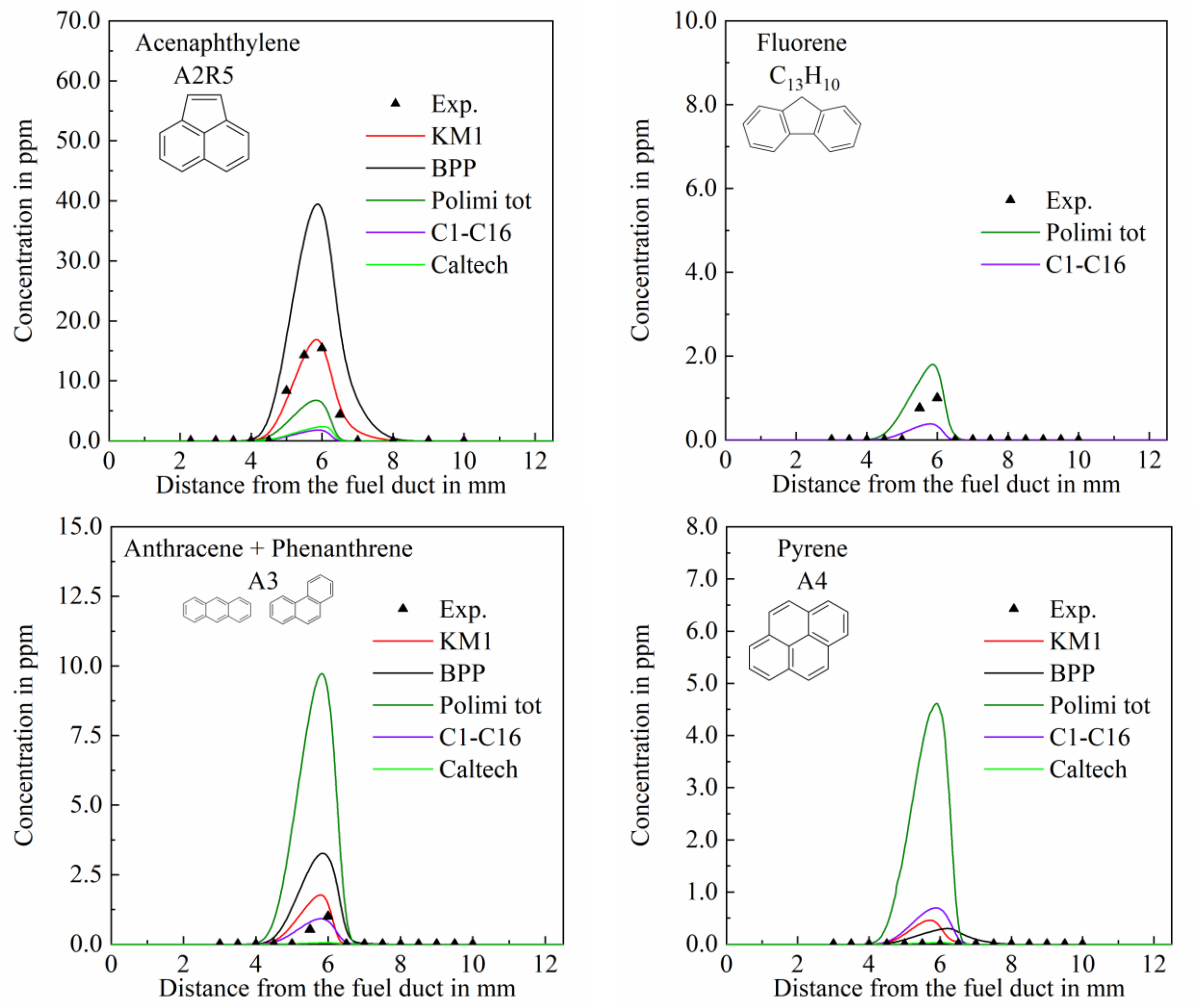

Figure 24: Measured (symbols) and computed (solid lines) concentration profiles of PAHs with more than one aromatic ring versus DFD in a non-premixed iso-octane counterflow flame.

All the above reflects the importance of the fundamental experiments in counterflow non-premixed flames for the ESTiMatE project in order to develop an accurate prediction model. In this context, many flames for different fuels have been investigated in order to facilitate the activity of the development of the chemical kinetic and soot models. In the following, experimental results gained from different iso-octane counterflow non-premixed flames with different fuel mass fractions and strain rates will be presented.

4.1.2 Influence of fuel mass fraction on flame structure and soot formation

In this part of the report the influence of fuel mass fraction is presented. For this purpose, temperature, gaseous species profiles and soot formation results from flame 1 to flame 4 from Table 3 will be presented. Scope of this part of the report is not only to present the influence of the fuel mass fraction and strain rate but mainly to highlight that the designed facilities and systems at the EBI-Vbt at the KIT are able to capture even small changes in the flames structure. Hence, in this part of the report the authors will not go in deep to explain the physics and chemistry behind the presented measurements, as this is going to be discussed in the reports of the developed models.

Figure 25 depicts radiation corrected temperature profiles gained from flames 1 – 4 (Y_F = 0.35, 0.47, 0.50 and 0.60 & a strain rate of 60 s^{-1}). From the measurements and the simulations it is clear that with increasing fuel mass fraction the flame's peak temperature and width are increasing. Furthermore, the flame's position is shifting toward the oxidizer duct. Both phenomena are captured well by the measurements showing the sensitivity of the temperature measurement device which is very important for the model development.

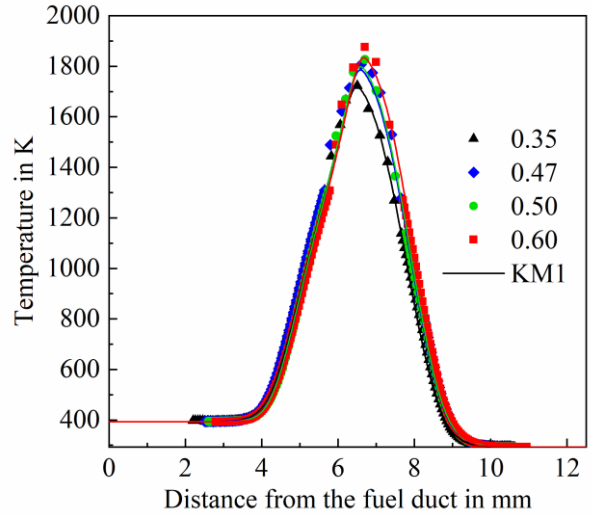

Figure 25: Radiation corrected temperature profiles of non-premixed iso-octane counterflow flames; Variation of fuel mass fraction from 0.35 to 0.6 at a constant strain rate of 60 s^{-1}.

The Influence of the fuel mass fraction on gaseous species concentration profiles is presented in Figure 26, Figure 27, Figure 28 and Figure 29. In all quantified species the influence of the fuel mass fraction could be detected. The increase of the concentration for all species is observed with increasing Y_F.

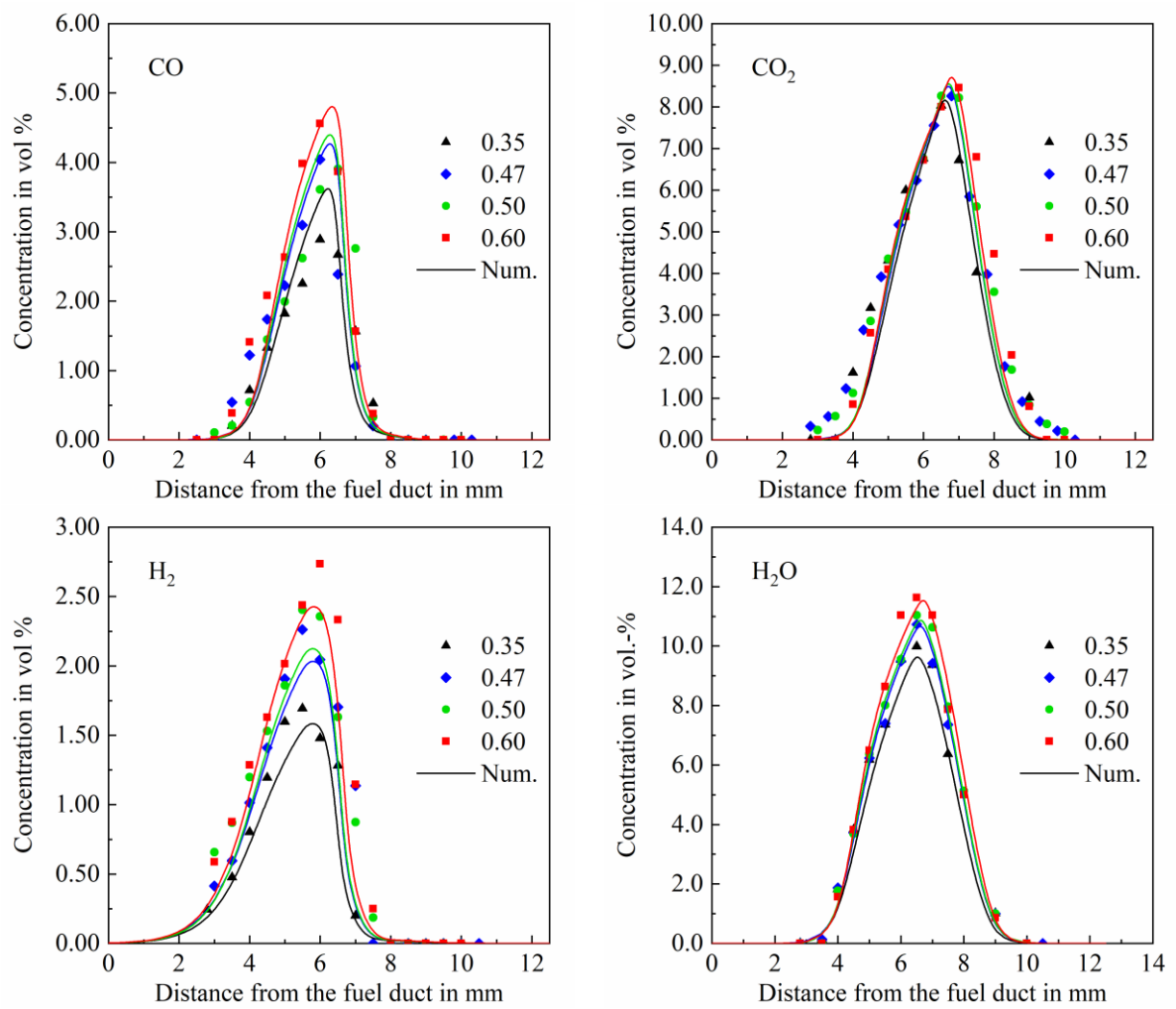

Figure 26: Measured (symbols) and computed (solid lines) concentration profiles of C_8H_{18}, O_2, N_2, CO_2, H_2O, CO and H_2 versus Distance from the Fuel Duct (DFD) in non-premixed iso-octane counterflow flames at a strain rate of 60 s^{-1} and fuel mass fractions of 0.35, 0.47, 0.50 and 0.60.

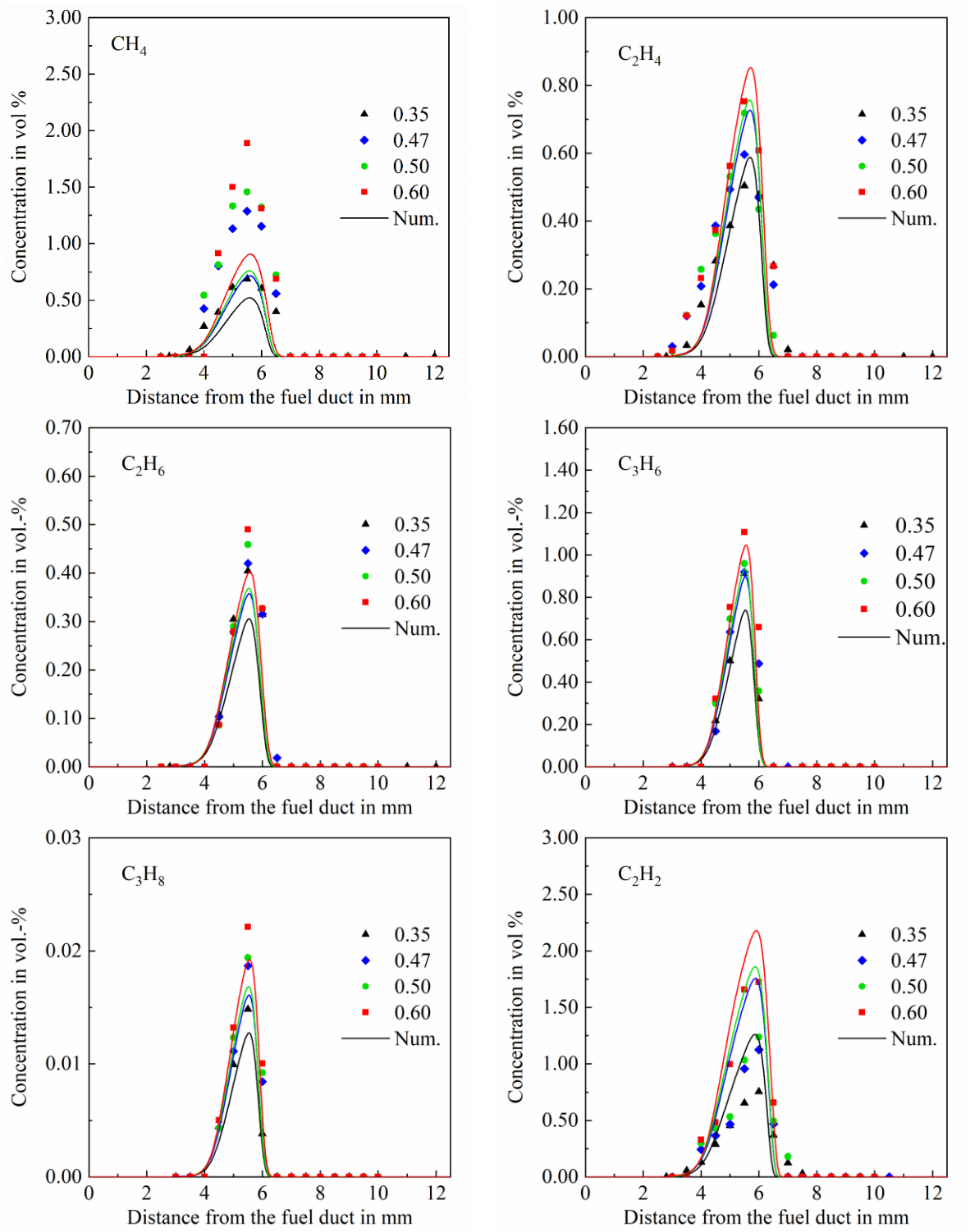

Figure 27: Measured (symbols) and computed (solid lines) concentration profiles of small hydrocarbons versus Distance from the Fuel Duct (DFD) in non-premixed iso-octane counterflow flames at a strain rate of 60 s^{-1} and fuel mass fractions of 0.35, 0.47, 0.50 and 0.60.

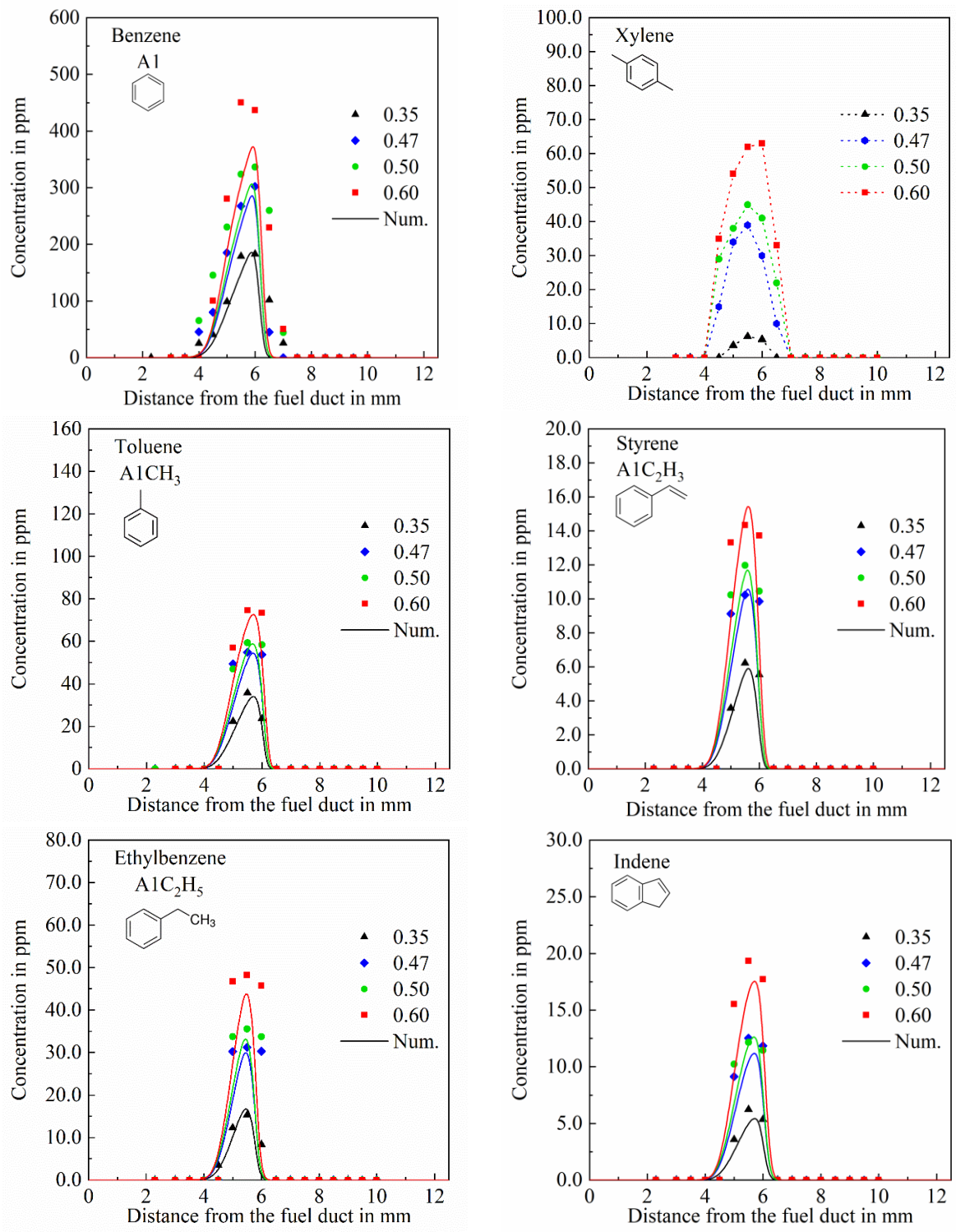

Figure 28: Measured (symbols) and computed (solid lines) concentration profiles of aromatics and PAHs versus Distance from the Fuel Duct (DFD) in non-premixed iso-octane counterflow flames at a strain rate of 60 s^{-1} and fuel mass fractions of 0.35, 0.47, 0.50 and 0.60.

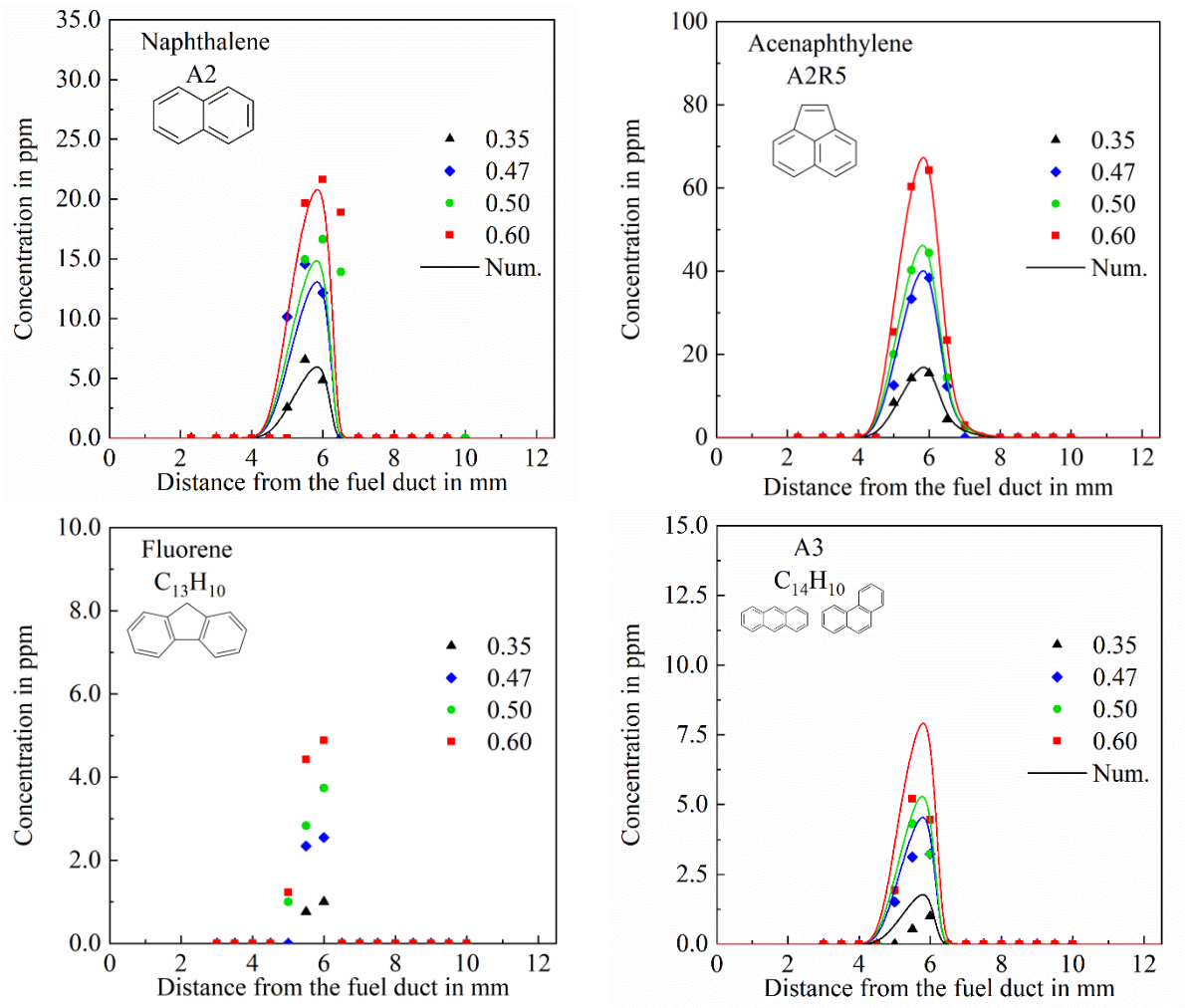

Figure 29: Measured (symbols) and computed (solid lines) concentration profiles of PAHs with more than one aromatic ring versus Distance from the Fuel Duct (DFD) in non-premixed iso-octane counterflow flames at a strain rate of 60 s^{-1} and fuel mass fractions of 0.35, 0.47, 0.50 and 0.60.

Soot formation

The last data to fulfil the data set of a flame are the data regarding the soot formation process. These data include the sooting limits of the counterflow flames for respectively fuel and the formed particles. The determined soot limit map for iso-octane in non-premixed configuration is presented in Figure 30. This map correlates the fuel mass fraction with the strain rate in order to now at which conditions (Y_F and α_2) a flame is sooty or not. In Figure 31 the determined soot volume fractions along the flame axes are presented for the flames 2 - 4 from Table 3. Data for flame 1 are not available as this flame is at non-sooting conditions and no soot could be detected in this flame. With the system developed for determining soot formation in the examined flames, also the primary particle distribution could defined. Exemplary the measured primary soot particle size distributions (PSPSDs) via LII in the non-premixed iso-octane counterflow flame with a fuel mass fraction of 0.47 and a strain rate of 60 s^{-1} are presented. The PSPSDs for all

investigated flames from Table 3 have been determined and shared with the project partner like all data presented in this report to facilitate the development of the models.

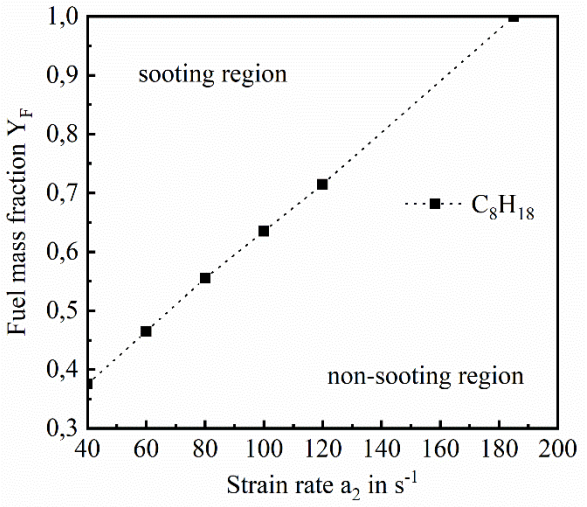

Figure 30: Sooting limit map of iso-octane non-premixed counterflow flames

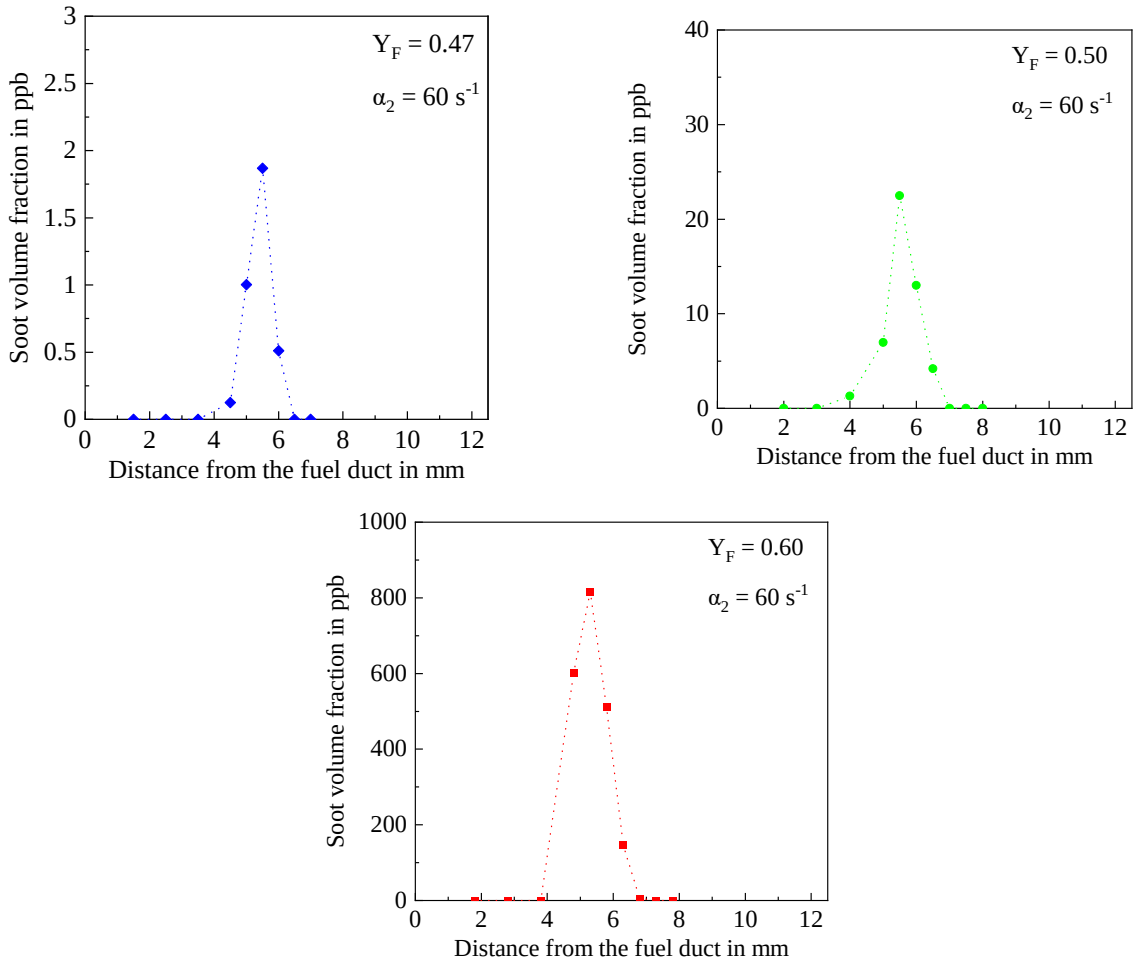

Figure 31: Measured soot volume fraction versus DFD in non-premixed iso-octane counterflow flames at a strain rate of 60 s^{-1} and fuel mass fractions of 0.47, 0.50 and 0.60.

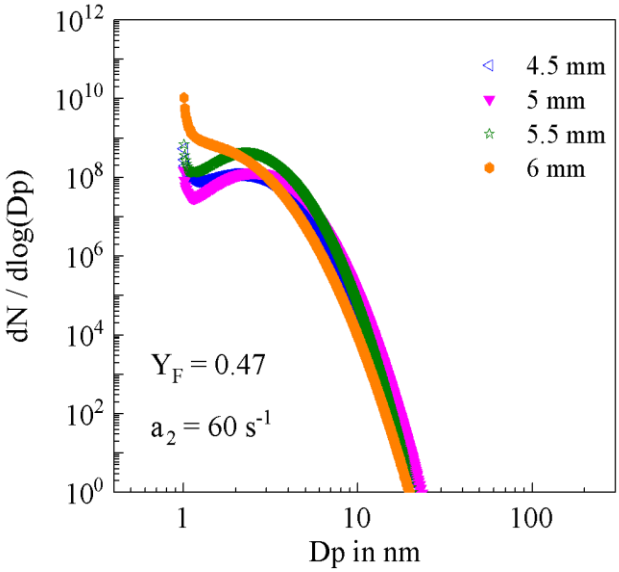

Figure 32: Determined primary soot particle size distributions SPSDs via LII in a non-premixed iso-octane counterflow flame at a fuel mass fraction of 0.47 and a strain rate of 60 s^{-1} (at the soot limit).

4.1.3 Influence of strain rate on flame structure and soot formation

Similar to the flames presented in the last sub-chapter, this part of the report shows the influence of the strain rate on flame structure and soot formation in iso-octane non-premixed counterflow flames. Figure 33 depicts the measured temperature profiles in flames 4-6. This plot shows clearly that the decreasing effect of the strain rate on temperature can be measured well. Additionally, the decrease of the width of the flame with increasing strain rate could also be accurately detected.

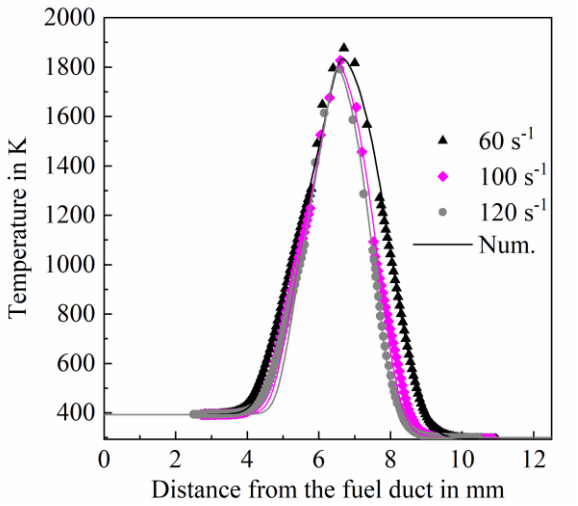

Figure 33: Radiation corrected temperature profiles of non-premixed iso-octane counterflow flames at a fuel mass fraction of 0.6 and stain rates from 60 s^{-1} to 120 s^{-1}.

Similarly, as in the previous section data regarding the influence of strain rate on gaseous

species concentrations are presented. All species determined in these flames and their concentration profiles are presented in Figure 34, Figure 35, Figure 36 and Figure 37. From the measured results it is clear that, by increasing the strain rate from 60 s^{-1} to 120 s^{-1} the peak concentration of all the higher hydrocarbons (>C5) and PAHs decreases, while the peak concentration of the major species like CO_2 and H_2O seems not to be affected. Additionally, from all measured concentration profiles the decrease in the width of the flame by increasing the strain rate could be observed. This comes into agreement with the results of the temperature measurements. In this point the authors want to highlight the ability of the system to capture not only the changes in the concentrations but also the differences in the width of the flame even for a small increase in the strain rate of 20 s^{-1}.

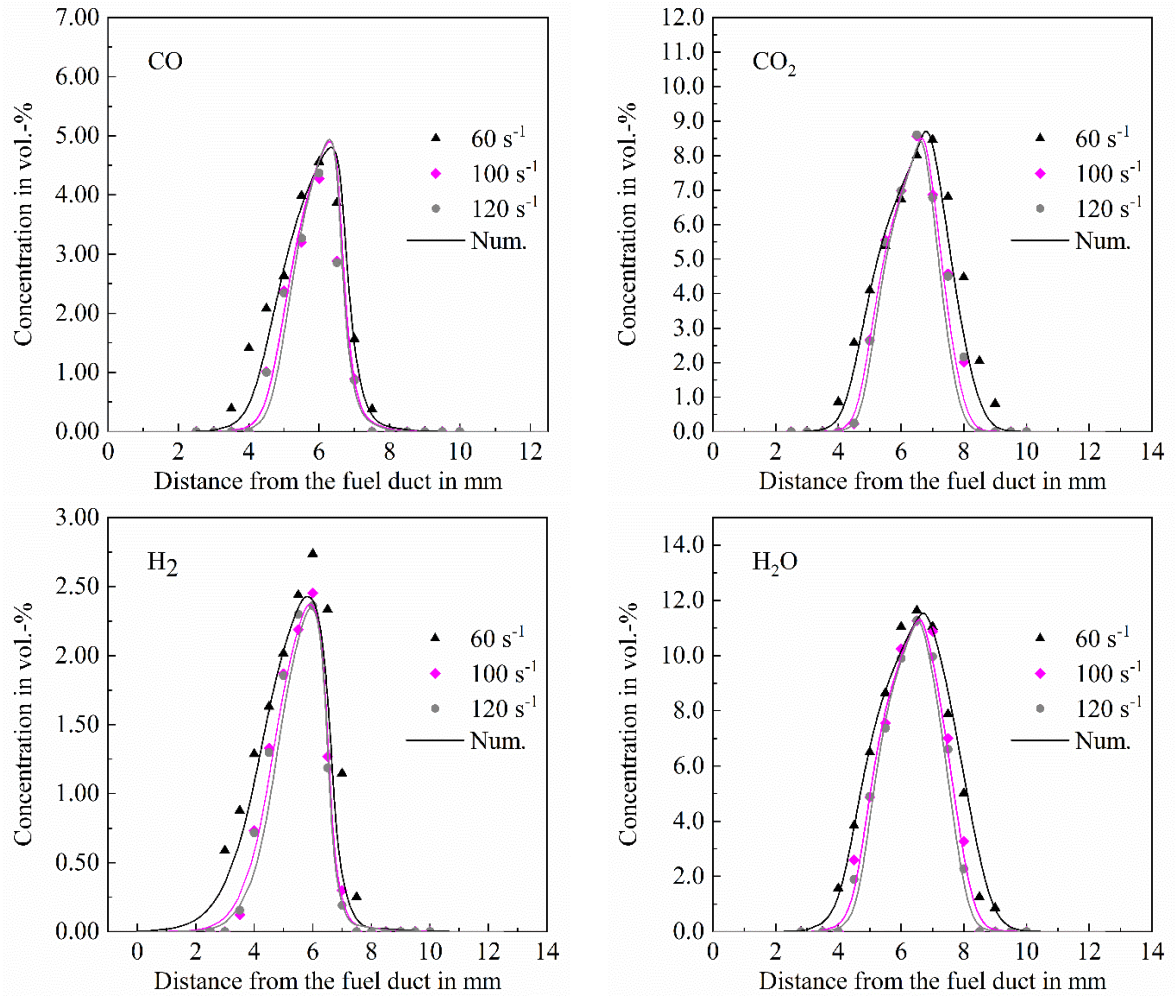

Figure 34: Measured (symbols) and computed (solid lines) concentration profiles of C_8H_{18}, O_2, N_2, CO_2, H_2O, CO and H_2 versus Distance from the Fuel Duct (DFD) in non-premixed iso-octane counterflow flames at a strain rate of 60 s^{-1} and fuel mass fractions of 0.35, 0.47, 0.50 and 0.60.

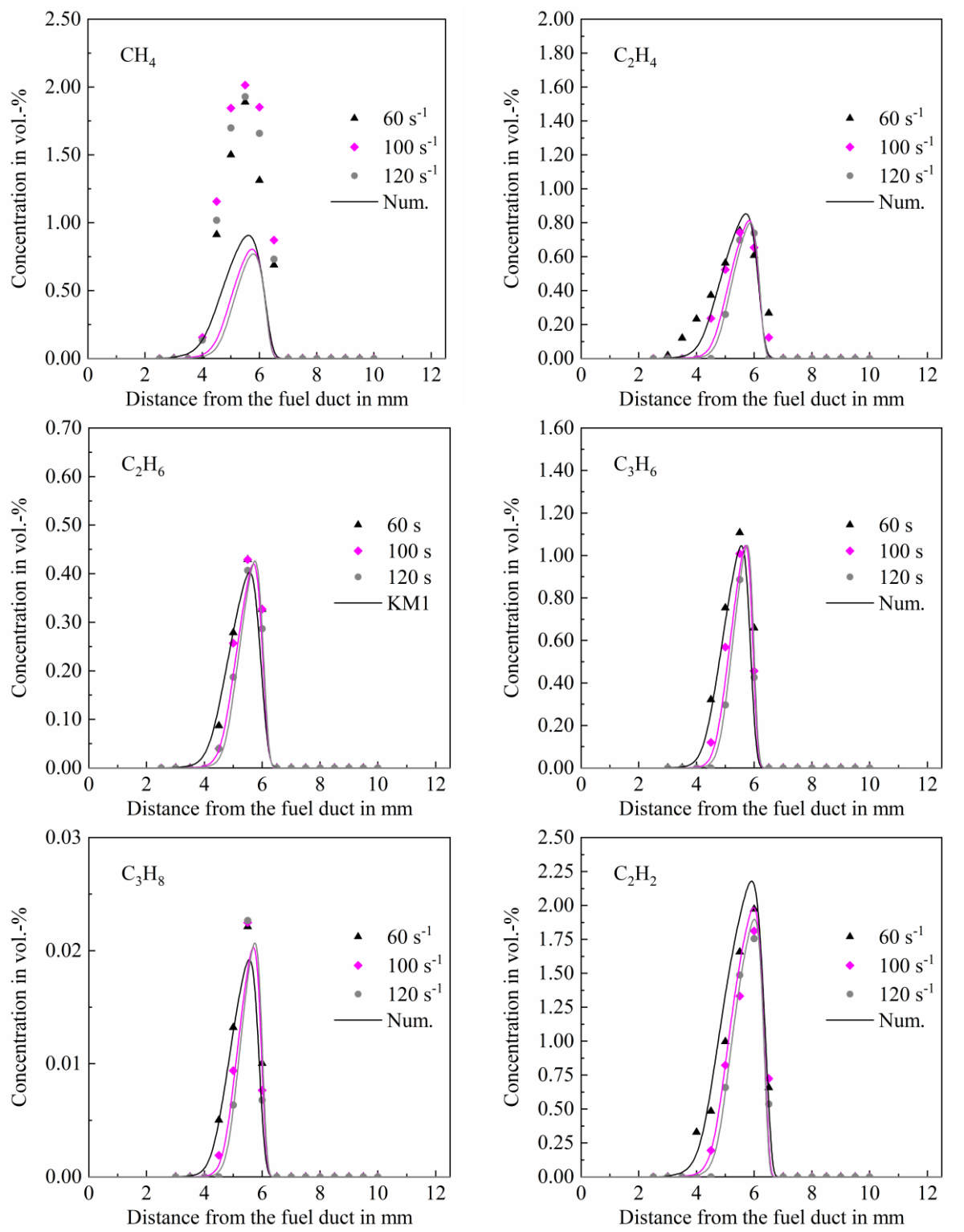

Figure 35: Measured (symbols) and computed (solid lines) concentration profiles of small hydrocarbons versus Distance from the Fuel Duct (DFD) in non-premixed iso-octane counterflow flames at a Y_F of 0.60 and strain rates of 60 s^{-1} , 100 s^{-1} and 120 s^{-1}.

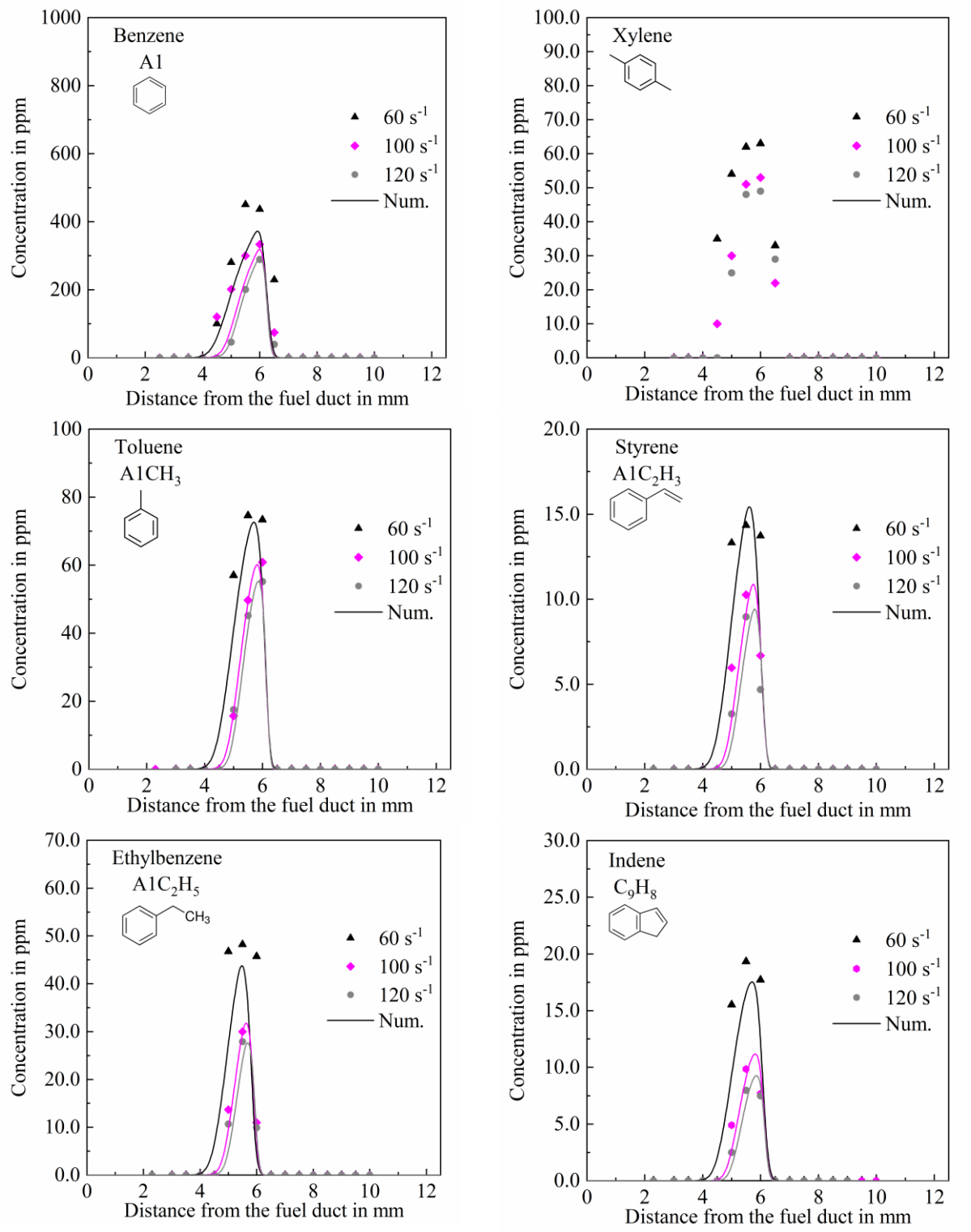

Figure 36: Measured (symbols) and computed (solid lines) concentration profiles of aromatics and PAHs versus Distance from the Fuel Duct (DFD) in non-premixed iso-octane counterflow flames at a Y_F of 0.60 and strain rates of 60 s^{-1} , 100 s^{-1} and 120 s^{-1}.

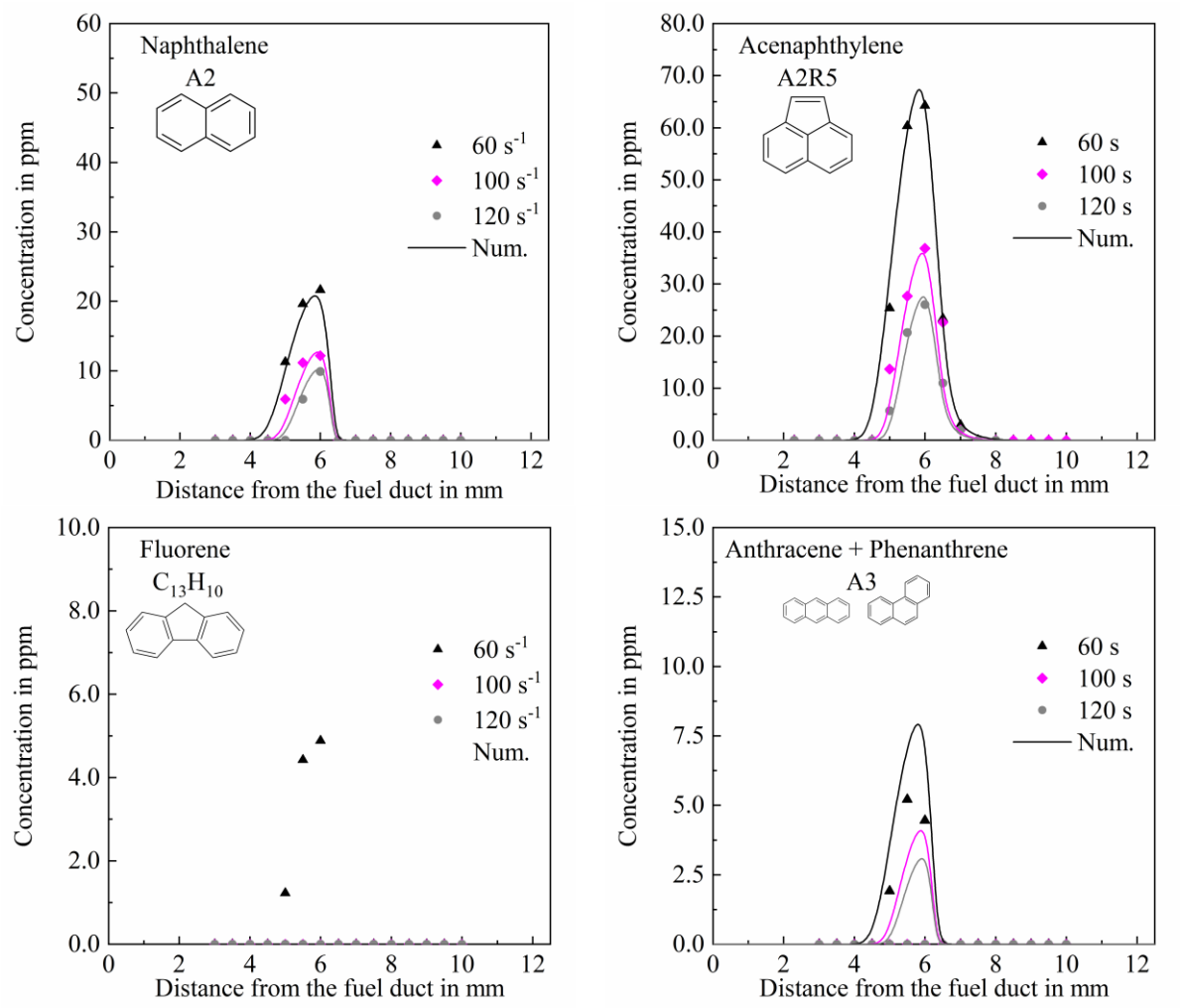

Figure 37: Measured (symbols) and computed (solid lines) concentration profiles of PAHs with more than one aromatic ring versus Distance from the Fuel Duct (DFD) in non-premixed iso-octane counterflow flames at a Y_F of 0.60 and strain rates of 60 s^{-1} , 100 s^{-1} and 120 s^{-1}.

Soot formation

Flames 5 and 6 that are used here to show the influence of strain rate on flame temperature and species concentration profiles are non-sooting flames. Thus, no soot could be detected in these flames. In order be able to generate data showing the influence of strain rate on soot formation two additional flames at lower strain rates, shown on Table 5, have been investigated. The measured soot volume fraction in flames 4, 7 & 8 are presented in Figure 38. Similar to the concertation of the PAHs, the concentration of the soot particles decreases significantly by increasing the strain rate. The graphs below show that even a small increase in the stain rate from 60 s^{-1} to 80 s^{-1} reduces the soot concentration by at least one order of magnitude.

Table 5: Investigated flames for the determination of the influence of strain rate on soot formation

Iso-octane non-premixed flames					
		Fuel side		Oxidizer side	
Flames	α_2 (s^{-1})	$Y_{C8H18,1}$	$Y_{N2,1}$	$Y_{O2,2}$	$Y_{N2,2}$
4	60	0.60	0.40	0.233	0.767
7	70	0.60	0.40	0.233	0.767
8	80	0.60	0.40	0.233	0.767

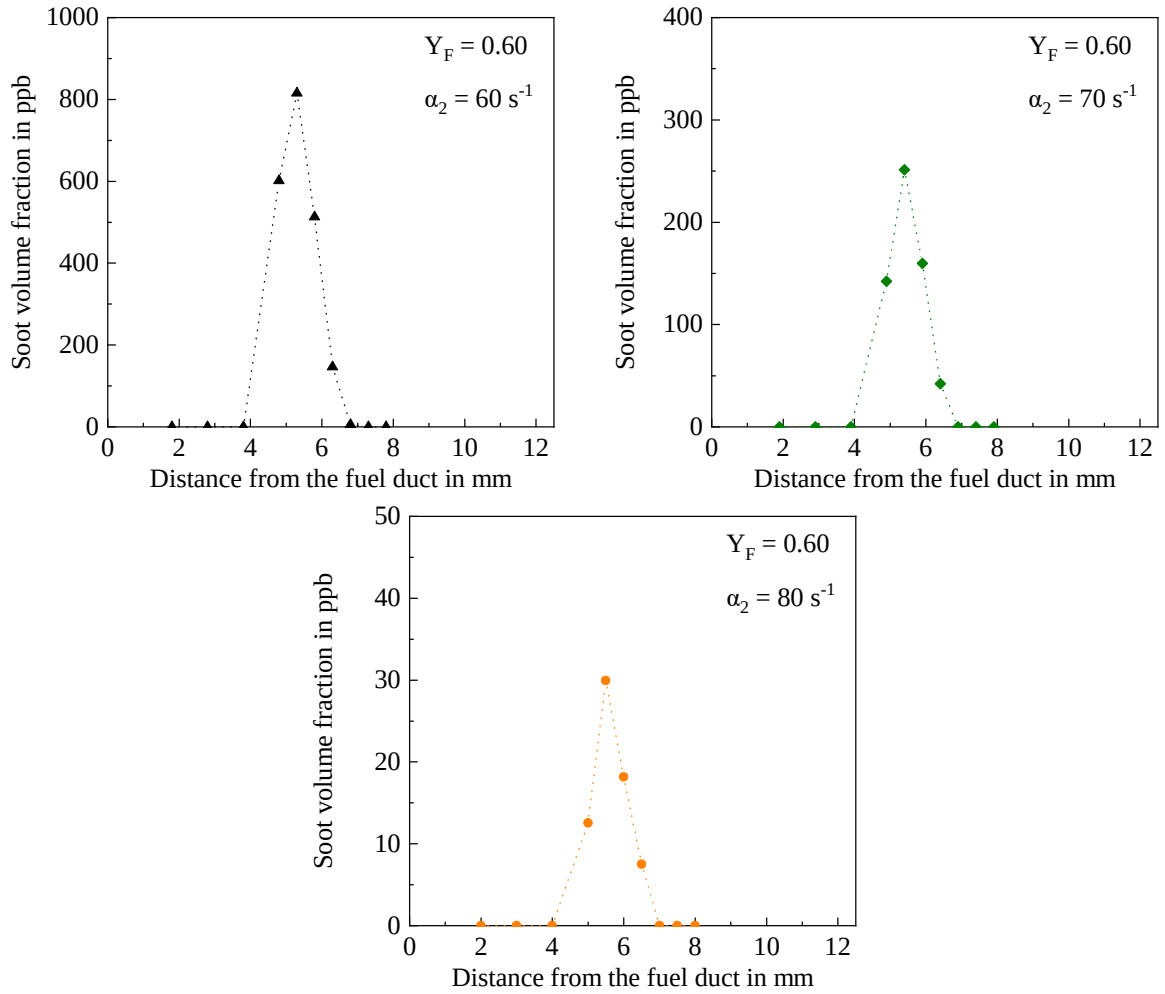

Figure 38: Measured soot volume fraction versus Distance from the Fuel Duct (DFD) in non-premixed iso-octane counterflow flames at a fuel mass fraction of 0.60 and strain rates of 60 s^{-1}, 70 s^{-1} and 80 s^{-1}.

4.2 Experimental matrix of non-premixed counterflow at atmospheric pressure

In order to generate a complete data set strong enough to facilitate the development and the validation of the chemical kinetic and soot models for a four component surrogate at the EBI-VBT at KIT more than 30 flames under atmospheric conditions for various fuels have been characterised regarding temperature field, gaseous species concentration profiles and soot formation. As all the data generated in W.P.5.1 will be used for the development of the respectively models, they will be reported in detail in the reports for the model development from the respectively partner. For this reason the authors present in this report only the table containing all the flames investigated in the framework of ESTiMatE. In the following tables all under atmospheric conditions investigated flames with the used fuel, their boundary conditions (Y_F & α_2) and the gained data are presented. I understand that you cannot present all the data, since that would be too much. However, it would be interesting to show some results of changing species concentration as function of the different fuels.

ISO-OCTANE FLAMES						
Flames	**FUEL**	**α_2 (s^{-1})**	**Temp. Meas.**	**Species Meas.**	**SOOT Measurements**	**Sooting/ non-sooting**
1	C_8H_{18}	60	√	√	√	NO SOOT
2	C_8H_{18}	60	√	√	√	SOOTING
3	C_8H_{18}	60	√	√	√	SOOTING
4	C_8H_{18}	60	√	-	√	SOOTING
5	C_8H_{18}	60	√	√	√	SOOTING
6	C_8H_{18}	70	√	-	√	SOOTING
7	C_8H_{18}	80	√	-	√	SOOTING
8	C_8H_{18}	100	√	√	√	NO SOOT
9	C_8H_{18}	120	√	√	√	NO SOOT

ETHYLENE FLAMES						
Flames	**FUEL**	**α_2 (s^{-1})**	**Temp. Meas.**	**Species Meas.**	**SOOT Measurements**	**Sooting/ non-sooting**
10	C_2H_4	60	-	-	√	SOOTING
11	C_2H_4	60	√	√	√	SOOTING
12	C_2H_4	60	√	√	√	SOOTING
13	C_2H_4	60	√	√	-	SOOTING
14	C_2H_4	40	-	-	√	SOOTING
15	C_2H_4	80	-	-	√	SOOTING
16	C_2H_4	100	√	√	√	NO SOOT
17	C_2H_4	120	√	√	√	NO SOOT

ETHYLENE FLAMES DOPED WITH THE SURROGATE A						
Flames	**FUEL**	**α_2 (s^{-1})**	**Temp. Meas.**	**Species Meas.**	**SOOT Measurements**	**Sooting/ non-sooting**
16	C_2H_4	100	√	√	√	NO SOOT
18	C_2H_4+2500ppm Surrogate A	100	√	√	√	SOOTING
19	C_2H_4+5000ppm Surrogate A	100	√	√	√	SOOTING

SURROGATE A FLAMES						
Flames	**FUEL**	**α_2 (s^{-1})**	**Temp. Meas.**	**Species Meas.**	**SOOT Measurements**	**Sooting/ non-sooting**
20	Surrogate A	60	√	√	√	NO SOOT
21	Surrogate A	60	√	-	√	SOOTING
22	Surrogate A	60	√	-	√	SOOTING
23	Surrogate A	60	√	√	√	SOOTING
24	Surrogate A	80	√	-	√	SOOTING
25	Surrogate A	90	√	√	√	SOOTING

TMB 1,3,5 FLAMES AND ETHYLENE & METHANE FLAMES DOPED WITH TMB 1,3,5						
Flames	**FUEL**	**α_2 (s^{-1})**	**Temp. Meas.**	**Species Meas.**	**SOOT Measurements**	**Sooting/ non-sooting**
16	C_2H_4	100	√	√	√	NO SOOT
26	C_2H_4 + 2500 ppm TMB 1,3,5	100	√	√	-	SOOTING
27	CH_4	100	√	√	√	NO SOOT
28	CH_4 + 2500 ppm TMB 1,3,5	100	√	√	-	SOOTING
29	TMB 1,2,4	60	√	√	-	SOOTING
30	TMB 1,2,4	60	√	√	-	SOOTING
31	TMB 1,3,5	60	√	√	-	SOOTING
32	C_2H_4 + 500 ppm TMB 1,3,5	100	√	√		NO SOOT

4.3 Experimental matrix of non-premixed counterflow under high pressure

In this part of the report the investigated non-premixed counterflow flames at high pressure, performed at EBI-Vbt at KIT will be presented. Like in the atmospheric flames, here only tables with the boundary conditions of the investigated flames will be presented, as the results will be discussed in detail in the respectively report of the model development.

The focus of the experimental campaign on high pressure flames is to determine the influence of pressure on flame structure. Hence, the high pressure setup presented in chapter 3.3 in used., Furthermoe, the developed probing system shown in 3.4 and the GC-MS system presented in 3.2.2 are applied.,The gaseous species concentration profiles were determined and shared in order to validate the chemical kinetic model at high pressure conditions. This step is essential for the performance of the model and especially for the development of the reduced model that will be developed out of the detailed one. Table 6 shows the investigated ethylene flames under high pressure. In the frame work of ESTiMatE it was decided to investigate flames at three different pressure levels (1, 2 & 5 bar). Additionally, with the set of flames presented in Table 6 the effect of pressure on the influence of the fuel mass fraction and strain rate can be determined and clarified.

Table 6: Investigated ethylene non-premixed counterflow flames at various Y_F and α_2 at 1 bar, 2 bar and 5 bar.

Non-premixed counterflow flames under pressure			
Fuel	**Strain rate**	**Fuel mass fraction**	**Pressure**
Ethylene	100 s^{-1}	0.125	1, 2 & 5
Ethylene	100 s^{-1}	0.15	1, 2 & 5
Ethylene	120 s^{-1}	0.15	1, 2 & 5
Ethylene	150 s^{-1}	0.15	1, 2 & 5

The sensitivity and the achieved resolution of species concentration profiles under high pressure conditions (5bar) is exemplary presented in Figure 39 based on results from an ethylene non-premixed flame with a fuel mass fraction of 0.125 and a strain rate of 100 s^{-1}. Following to that, the influence of pressure on the measured peak concentration of soot precursors is presented in Figure 40.

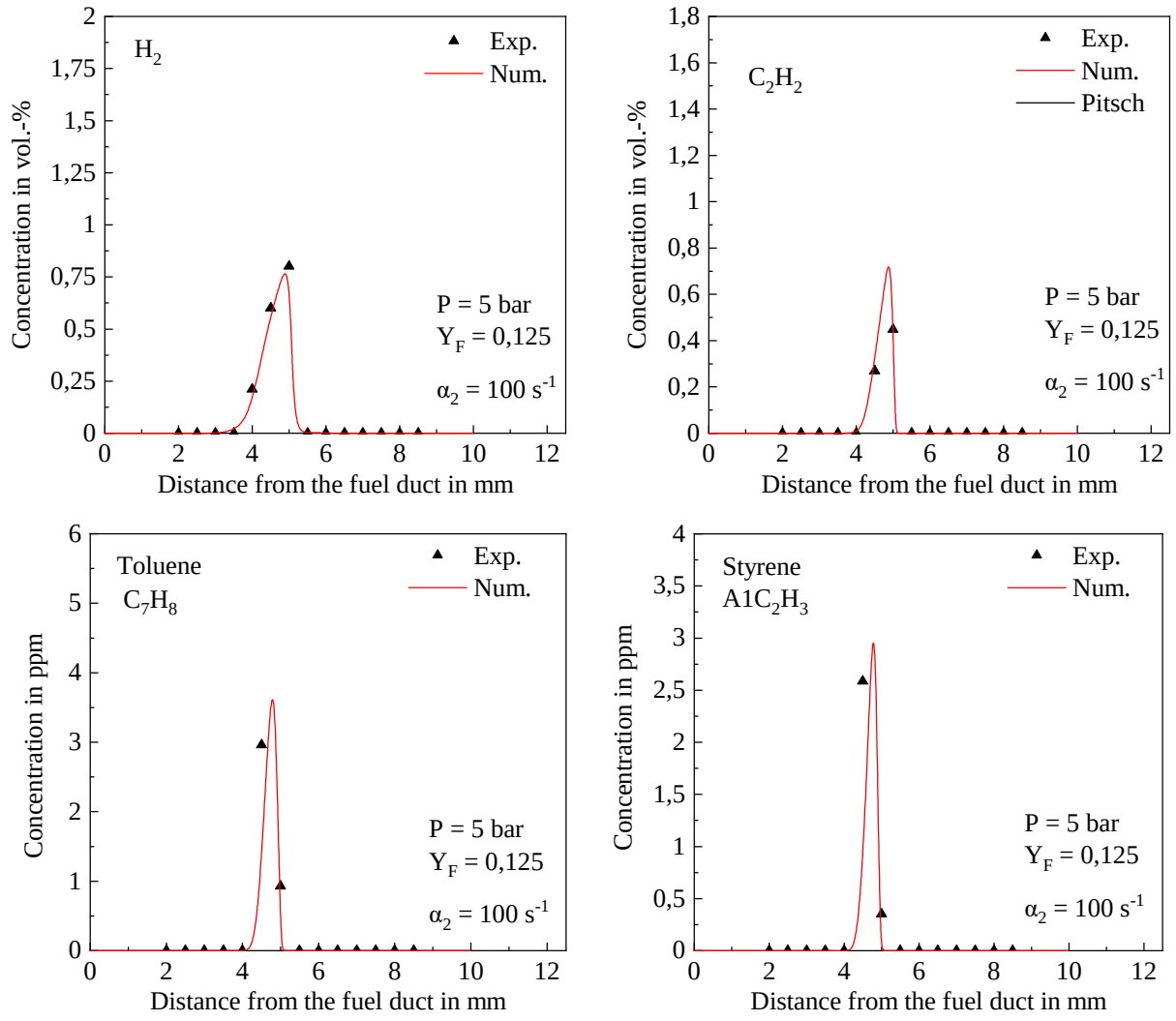

Figure 39: Measured (symbols) and computed (solid line) concentration profiles of H_2,C_2H_2, toluene and styrene versus Distance from the Fuel Duct (DFD) in a non-premixed ethylene counterflow flame at a pressure of 5 bar.

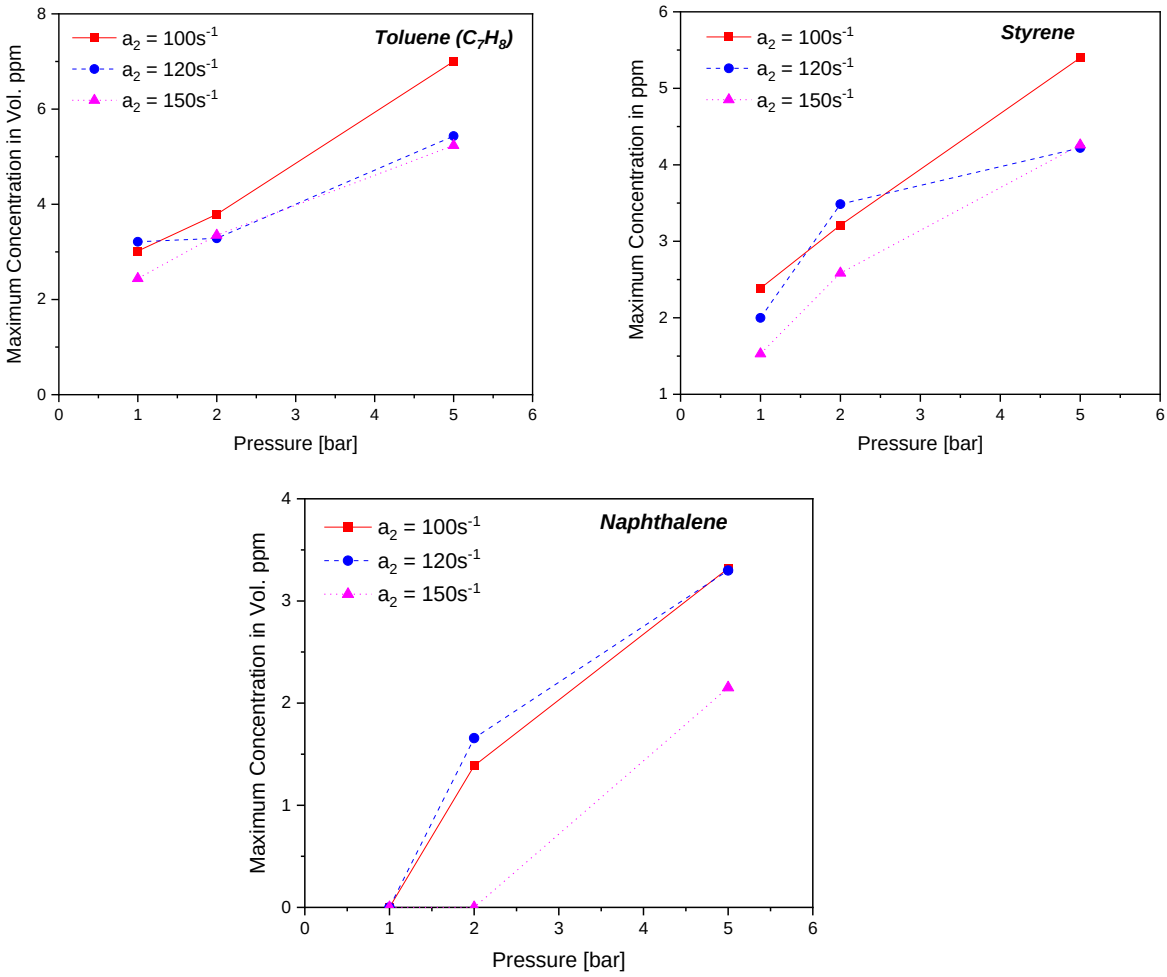

Figure 40: Measured peak concentrations of toluene styrene and naphthalene versus pressure in non-premixed ethylene counterflow flames.

Data from flames under pressure have to be generated also for the surrogate A. Due to technical problems and long delivery times, due to the pandemic situation we have been facing the last two years (the GC-MS system was defect for several months), the data regarding the surrogate flames have not been generated completely yet. However, EBI-Vbt is in close contact with the partners from USTUTT in order to deliver the required data. In cooperation with USTUTT, KIThave generated the experimental matrix with the surrogate A flames to be investigated under pressure (Table 7). All the problems leading to the reported delay have been solved and the campaign has started. EBI-Vbt will deliver the data to USTUTT in the upcoming months outside of the reporting period. The experimental data of the surrogate A flames will be uploaded to the ESTiMatE intranet like all the experimental data generated at EBI-Vbt at KIT in the reporting period.

Table 7: Investigated surrogate A non-premixed counterflow flames at various Y_F and α_2 at 1 bar, 2 bar and 5 bar.

Non-premixed counterflow flames under pressure			
Fuel	**Strain rate**	**Fuel mass fraction**	**Pressure**
Surrogate A	120 s^{-1}	0.10	1, 2 & 5
Surrogate A	150 s^{-1}	0.10	1, 2 & 5
Surrogate A	150 s^{-1}	0.125	5

5. Conclusions

Aim of the ESTiMatE project is the development of a modeling strategy for the prediction of soot particle emission from jet engines. In this context, a new chemical kinetic model and two soot models for a four component jet-surrogate fuel (surrogate A) will be developed and coupled in one 3-D CFD model. For the development and validation of the chemical kinetic and the soot models, investigations in 1-D model flames under well-defined boundary conditions uncoupled from engine complexity are essential. Additionally, the 1-D flame structure allows the application of detailed chemistry with low computational cost. Hence, at the EBI-Vbt at KIT fundamental investigation in 1-D non-premixed counterflow flames of ethylene, ethylene doped with the surrogate Jet-A and the pure surrogate Jet-A, at different pressure levels were performed. During the development of the chemical kinetic mechanism it was ascertained that, despite the investigations in ethylene and surrogate A flames, experimental data from flames of the single components of the surrogate A and especially from iso-octane and 1.3.5-trimethylbenzene are from higher importance due to lack of data in such flames. In this context, EBI-Vbt at KIT various measurements procedures and systems were developed for the detail characterization of the examined flames. For the temperature acquisition an in-house developed and constructed thermocouple with constant tension was used. All gaseous species profiles were determined via gas chromatography and the soot formation process in the flame was examined by using the laser scattering and the LII technique for the determination of the soot limits and soot formation (soot volume fraction & primary particle size distribution) respectively. In W.P.5.1, 32 flames under atmospheric conditions and
19 flames under high-pressure conditions were characterized in terms of temperature, gaseous species profiles and soot formation. The data generated in the W.P.5.1 were used for the development and validation of all sub chemical kinetic mechanisms and the final chemical kinetic model from USTUTT. Additionally, the soot data were used for the validation of the soot models.

References

[1] ICAO Environmental Report2016, https://www.icao.int/environmental-protection/Documents/EnvironmentalReports/2016/ENVReport2016_pg85-88.pdf

[2] A. K. Patra, S. Gautam, P. Kumarc, Emissions and human health impact of particulate matter from surface mining operation—A review, Environmental Technology & Innovation, volume 5, April 2016, Pages 233-249, doi: 10.1016/j.eti.2016.04.002

[3] German Aerospace Center, Lower soot emissions from aviation, DLR researchers understand soot formation in engines, 2019, https://www.dlr.de/content/en/articles/news/2019/01/20190326_researchers-understand-soot-formation-engines.html

[4] U. Niemann, K. Seshadri, FA. Williams. Accuracies of laminar counterflow flame experiments. Combustion and Flame 2015;162:1540–9. doi:10.1016/j.combustflame.2014.11.021.

[5] S. Ahuja and D. L. Miller Design of a constant tension thermocouple rake suitable for flame studies, Review of Scientific Instruments, Volume 64, Issue 5, 1358–1359, 1998, doi: 10.1063/1.1144093

[6] CR. Shaddix, Correcting thermocouple measurements for radiation loss: a critical review. Proceedings of the 33rd National Heat Transfer Conference, 1999.

[7] Joo PH, Wang Y, Raj A, Chung SH. Sooting limit in counterflow diffusion flames of ethylene/propane fuels and implication to threshold soot index. Proceedings of the Combustion Institute 2013;34:1803–9. doi:10.1016/j.proci.2012.06.124.

[8] Wang Y, Chung SH. Effect of strain rate on sooting limits in counterflow diffusion flames of gaseous hydrocarbon fuels: Sooting temperature index and sooting sensitivity index. Combustion and Flame 2014;161:1224–34. doi:10.1016/j.combustflame.2013.10.031.

[9] Raj A, Prada IDC, Amer AA, Chung SH. A reaction mechanism for gasoline surrogate fuels for large polycyclic aromatic hydrocarbons. Combustion and Flame 2012;159:500–15. doi:10.1016/j.combustflame.2011.08.011.

[10] Blanquart G, Pepiot-Desjardins P, Pitsch H. Chemical mechanism for high temperature combustion of engine relevant fuels with emphasis on soot precursors. Combustion and Flame 2009;156:588–607. doi:10.1016/j.combustflame.2008.12.007.

[11] Zhong B-J, Zheng D. Chemical Kinetic Mechanism of a Three-Component Fuel

Composed of Iso-octane/ n -Heptane/Ethanol. Combustion Science and Technology 2013;185:627–44. doi:10.1080/00102202.2012.739223.

[12] Frassoldati A, Cuoci A, Faravelli T, Ranzi E. Kinetic Modeling of the Oxidation of Ethanol and Gasoline Surrogate Mixtures. Combustion Science and Technology 2010;182:653–67. doi:10.1080/00102200903466368.

[13] Pelucchi M, Cavallotti C, Faravelli T, Klippenstein SJ. H-Abstraction reactions by OH, HO 2 , O, O 2 and benzyl radical addition to O 2 and their implications for kinetic modelling of toluene oxidation. Physical Chemistry Chemical Physics 2018;20:10607–27. doi:10.1039/C7CP07779C.

[14] Ranzi E, Frassoldati A, Grana R, Cuoci A, Faravelli T, Kelley AP, et al. Hierarchical and comparative kinetic modeling of laminar flame speeds of hydrocarbon and oxygenated fuels. Progress in Energy and Combustion Science 2012;38:468–501. doi:10.1016/j.pecs.2012.03.004.

[15] Blanquart G. Effects of spin contamination on estimating bond dissociation energies of polycyclic aromatic hydrocarbons. International Journal of Quantum Chemistry 2015;115:796–801. doi:10.1002/qua.24904.